REPUBLIC OF TÜRKİYE
ADANA ALPARSLAN TÜRKEŞ SCIENCE AND TECHNOLOGY UNIVERSITY

GRADUATE SCHOOL
AERONAUTICAL AND SPACE SCIENCES DEPARTMENT

INVESTIGATION ON THE EFFECTS OF DIELECTRIC MATERIAL ON THE THRUST PERFORMANCE OF ANNULAR DBD PLASMA ION THRUSTERS

AYHAN ALP ÇETİNKAYA

M.Sc.

ADANA 2023

REPUBLIC OF TÜRKİYE
ADANA ALPARSLAN TÜRKEŞ SCIENCE AND TECHNOLOGY UNIVERSITY

GRADUATE SCHOOL
AERONAUTICAL AND SPACE SCIENCES DEPARTMENT

INVESTIGATION ON THE EFFECTS OF DIELECTRIC MATERIAL ON THE THRUST PERFORMANCE OF ANNULAR DBD PLASMA ION THRUSTERS

AYHAN ALP ÇETİNKAYA

M.Sc.

THESIS ADVISOR
ASST. PROF. DR. HÜRREM AKBIYIK

ADANA, 2023

DECLARATION OF CONFORMITY

In this thesis study, which was prepared following the thesis writing rules of Adana Alparslan Türkeş Science and Technology University Institute of Graduate School, I declare that I provide all the information, documents, evaluations and results in accordance with scientific ethics and moral codes without resorting to any means or assistance that would be contrary to scientific ethics and traditions. I also declare that I refer to all of the articles I used in this study with appropriate references and accept all moral and legal consequences if a situation is found contrary to my statement regarding my work.

21/12/2023

Ayhan Alp ÇETİNKAYA

ÖZET

DİELEKTRİK MALZEMENİN HALKALI DBD PLAZMA İYON İTİCİLERİN İTKİ PERFORMANSI ÜZERİNE ETKİLERİNİN İNCELENMESİ

Ayhan Alp ÇETİNKAYA
Yüksek Lisans, Havacılık ve Uzay Mühendisliği Anabilim Dalı
Danışman: Dr. Öğr. Üyesi Hürrem AKBIYIK
Aralık 2023, 72 sayfa

Bu tez çalışmasında, dielektrik malzemenin annular şeklindeki DBD plazma iyon iticilerinin itki performansı üzerindeki etkileri araştırılmıştır. Kısaca elektrik itki sistemi tarihçesi, elektrik itici tipleri ve DBD iyon iticileri hakkında bilgi verilmiştir. Yapılan çalışmalarda itki performansını en üst düzeyde tutabilmek için geometrik parametreler (annular ve sinusoidal), elektriksel parametreler ve malzeme türleri ele alınarak deneyler yapılmıştır.

Bütün yapılan deneylerde sırasıyla 4 kV_{pp}, 6 kV_{pp} ve 8 kV_{pp} voltajlar uygulanmıştır. Deneyler sırasında DBD plazma aktüatörü tarafından üretilen itki değerini ölçmek için ise elektronik itki ölçer cihazı kullanılmıştır. Yapılan deneyler sonucunda voltaj arttırıldıkça thrust değerinin arttığı gözlemlenmiştir. Ayrıca, aynı dış çapa sahip sinüs geometrilerinde çap arttıkça thrust etkinliğinin azaldığı gözlemlenmiştir.

Anahtar Kelimeler: İyon itici, Plazma aktüatör, Dielektrik malzeme, Halkalı iyon itici

ABSTRACT

INVESTIGATION ON THE EFFECTS OF DIELECTRIC MATERIAL ON THE THRUST PERFORMANCE OF ANNULAR DBD PLASMA ION THRUSTERS

Ayhan Alp ÇETİNKAYA
M.Sc., Department of Aeronautical and Space Sciences
Supervisor: Asst. Prof. Dr. Hürrem AKBIYIK
December 2023, 72 pages

In this thesis, the effects of dielectric material on the propulsion performance of annular DBD plasma ion thrusters are investigated. Briefly, the history of electric propulsion system, types of electric thrusters and DBD ion thrusters are given. In order to maximize the propulsion performance, geometrical parameters (annular and sinusoidal), electrical parameters and material types were considered and experiments were carried out.

In all experiments, voltages of 4 kV_{pp}, 6 kV_{pp} and 8 kV_{pp} were applied respectively. An electronic thrust measurement device was used to measure the thrust generated by the DBD plasma actuator during the experiments. As a result of the experiments, it is stated that the thrust value increases while the voltage is increased. Moreover, it is observed that for sine geometries with the same outer diameter, the thrust efficiency decreases as the diameter increases.

Keywords: Ion thruster, Plasma actuator, Dielectric material, Annular ion thruster

Dedication

To all researches who willing to study in this field.

ACKNOWLEDGEMENTS

I would like to thank my respected supervisor, Asst. Prof. Dr. Hürrem AKBIYIK, from the faculty of Aerospace and Aeronautical Engineering, Alparslan Türkeş Science and Technology University, whose worthy guidance, and professional attitude are appreciable in completing this thesis. It was a great privilege and honor to work and study under his guidance. He pushed me along this road and gave me the impression that I could always do better. Words alone cannot express my thanks to him for this as well.

I would like to thank my esteemed colleague Res. Asst. Remzi Can YILMAZ, Büşra KARATAŞ, Emircan BABAT, Ümmü Seleme ÖZLEN for his support in the preparation of this thesis. I am also thankful to my friend Gizem YILMAZ, Hasan AVCI who always support me.

I am grateful for my parents whose constant love and support keep me motivated and confident. I would like to thank my father Hamit ÇETİNKAYA, my mother Yıldız ÇETİNKAYA my sisters Sakine ÇETİNKAYA, Büşra ÇETİNKAYA BİRDAL and my brother Hakan BİRDAL who always supported me during my studies. My accomplishments and success are because they believed in me. My Deepest thanks to my siblings, who keep me grounded, remind me of what is important in life, and are always supportive of my adventures.

This thesis study is supported by the Scientific and Technological Research Council of Turkey (TUBITAK)—Grant No. 122M667.

TABLE OF CONTENTS

LIST OF FIGURES

LIST OF TABLES

LIST OF ABBREVIATIONS

kV_{pp}	: Peak-to-peak kilovoltage
kHz	: Kilohertz
Hz	: Hertz
mm	: Milimeter
D	: Annular diamater
d	: Radius of one side of the sinusoidal geometry
V_{pp}	: Peak-to-peak voltage
f	: Excitation frequency
HV	: High voltage
RF	: Radio frequency
Xe	: Xenon
ε	: Dielectric constant
t	: Dielectric material thickness

LIST OF SYMBOLS

SDBD	**:** Single dielectric barrier discharge
EP	**:** Electric propulsion
SERT-1	**:** Space electric rocket test-1
SMART-1	**:** Small missions for advanced research in technology-1
ET	**:** Electric thruster
MPD	**:** Magnetoplasmadynamic
FEEP	**:** Field effect electric propulsion
DBD	**:** Dielectic barrier discharge
MHD	**:** Magnetohydrodynamic
EHD	**:** Electrohydrodynamic
ns-DBDPA	**:** Nanosecond dielectric barrier discharge plasma actuator
AC	**:** Alternating current
DC	**:** Direct current
MUE	: Mass utilization efficiency
HDPE	: High density polyethylene

1. INTRODUCTION

In recent years, the use of single dielectric barrier discharge (SDBD) plasma ion thrusters has become widespread in both aerospace and aeronautics due to their ability to generate electrical impulse by interacting with air pressure in the field of flow control. SDBD usually has two electrodes, one of them is exposed and the other one is embeded, and a dielectric material is placed between these two electrodes. These electrodes are used usually linear or annular. Especially in the wings, linear electrodes are used to improve aerodynamic performance by reducing drag and increasing lift force, while annular electrodes are used in the space field because they produce a circular jet flow (Moreau, 2007). When high voltage is applied, the flow on the electrode in contact with the air releases ion winds towards the embedded electrode and forms the ion thruster. While this ion thruster has an alternative potential among propulsion devices due to its many advantages such as its ability to operate without any moving mechanism, fast response time, low weight and non-complex structure, it has some limitations in terms of working life. In this context, researchers are working on annular type ion thrusters, which are especially used in space, to improve their performance and extend their lifetime. In order to improve the performance of ion thrusters, these studies have generally focused on their geometrical properties (Akbıyık et al., 2018), electrical properties (Benard et al., 2014), the material of the electrode and dielectric (Stephen et al., 2014). One of the most important properties that have been investigated to extend the lifetime and improve the performance of the SDBD plasma actuator is the thickness and number of layers of the dielectric material used.

1.1. Electric Propulsion Systems History

Looking at the history of electric propulsion (EP), the first studies date back to the late 19th century, and it was the Russian scientist Konstantin Tsiolkovsky who first introduced the EP concept in the early 20th century (Kosmodemyansky, 2000). In his published work, Konstantin suggested that it would be possible to accelerate the particles by electrifying the particles coming out of the rocket in the future. In the same years, American physicist Robbert H. Goddard conducted a research and experiments on electrical particles. By confining electrical particles to a magnetic field, Robert wanted to greatly increase the probability of their collision with neutral molecules. Robert laid the foundation of EP by building the world's first electrostatic ion accelerator (Clary, 2003; Goddard, 1915). H. Oberth was the first to explain the concept of EP to people by relating it to space in his book published in 1929 (Oberth et al., 1923).

Despite all these proposals and studies, the systematic development of EP dates back to the 1950s. Ernst Stuhlinger, who derived rocket equations influenced by Jakob Ackeret's paper "On the Theory of Rockets", found the ratio of fuel mass to total initial mass (3.92) (Ackeret, 1947). More importantly, Stuhlinger showed that the energy conversion factor and propulsion systems are independent of all other parameters. During the years of the Second World War, L.R. Shepherd and A.V. Cleaver published a paper in which they explained the possibility of using nuclear energy to heat the propellant to meet the requirements of the rocket (Langmuir, 1913). In their studies, Shepherd and Cleaver suggested that EP-powered spacecraft could travel faster and therefore could be used in space exploration. The Space Electric Rocket Test (SERT 1) mission organized by NASA demonstrated the applicability of EP in space (Huang et al., 2012). In the 1965s, studies were reduced as it was realized that nuclear fuels were heavier than anticipated and that EP would take too much time to develop.

The use of hall thrusters to accelerate ions dates back to the 1970s. During these years, the Soviet Union made significant progress in the field of hall thrusters, although the United States took a tough stance against the research of hall thrusters (Choueiri et al., 2004). Towards the end of the 1990s, NASA's Deep Space 1 mission was able to successfully use the ion engine in space for the first time . In 2003, the European Space Agency's SMART-1 spacecraft used an ion engine to reach the Moon (Foing et al., 2003). With all these studies, ion thrusters have developed rapidly in the last 20 years and have been used in airplanes, communications, commercial satellites, space exploration and deep space missions.

1.2. Electric Thruster Types

Electric thruster (ET) is a system that uses electric charges to accelerate ions and to generate thrust. Many methods are used to generate this thrust. Among these methods, electron bombardment is a common method used in many space propulsion vehicles to ionize the propellant. The gas ionized by electron bombardment is accelerated using an electric field so that the vehicle can generate thrust in the opposite direction, thus generating thrust (Goebel et al., 2008). ET can be divided into 3 categories; electrothermal, electrostatic and electromagnetic as shown in Figure 1.

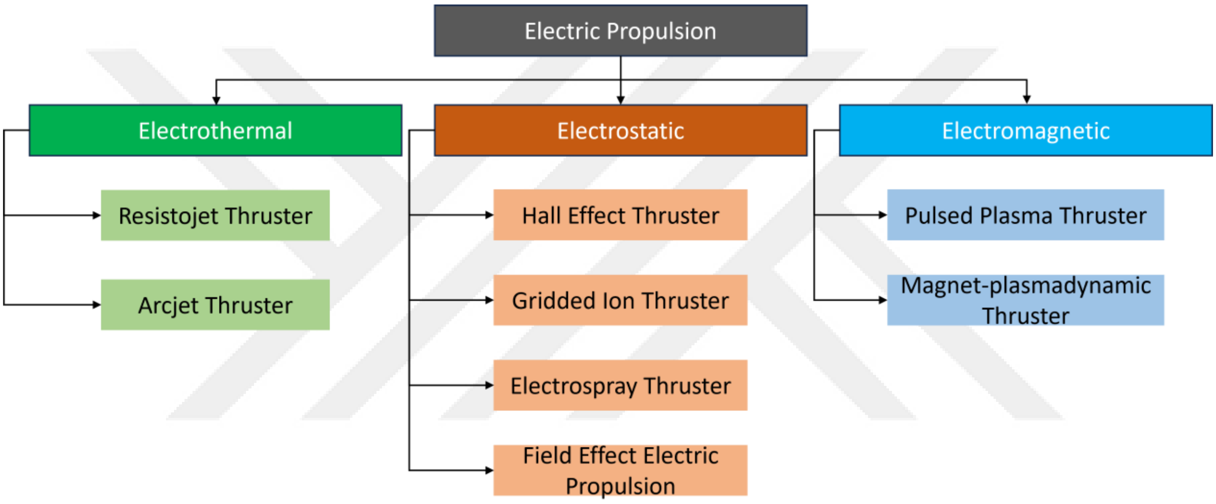

Figure 1. Classification of electric propulsion

1.2.1 Resistojet Thruster

Resistojet thruster is a type of electrothermal propulsion in which the propellant is heated by an electric heater. By increasing the temperature of the fluid used, the available output speed can be increased, but may not be sufficient for propulsion efficiency. Since they generally have low impulse values, they are not widely used in missions requiring long duration and high maneuverability.

1.2.2 Arcjet Thruster

It is the propulsion force generated by ionizing and accelerating the fluid flowing through a pipe, usually placed between two electrodes, with the help of an electric current and spraying it backwards. The force of this sprayed gas provides a thrust for the spacecraft. It is used in deep space missions with many advantages such as its sensitive maneuvering capabilities and low weight.

1.2.3 Pulsed Plasma Thruster

Consisting of an anode and a cathode, a pulsed plasma thruster generates thrust by transferring the energy of a high-voltage charged capacitor connected to the coil. Pulsed plasma thrusters use plasma pulses to accelerate the gas to high speeds and generate thrust. Pulsed plasma thrusters are an ideal propulsion system for small satellites and space exploration.

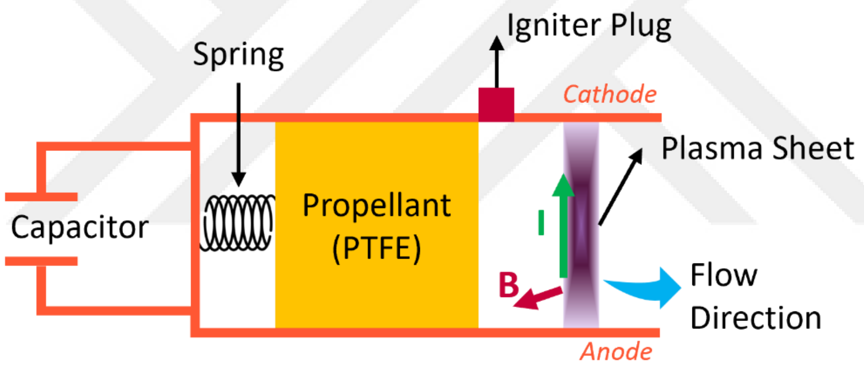

Figure 2. Schematic of pulsed plasma thruster

Figure 2 shows that the working principle of the pulsed plasma thruster. Here, the form in the intermittent region depending on the changing volume is shown as I current. Assuming that the current density is homogeneously distributed over the layer, only the integral current from the capacitors is considered to depend on I. B is the magnetic flux density. The relationship between B can be explained as follows.

$$B = \frac{\mu_0 I}{d}$$

1.2.4 Magneto-Plasmadynamic Thruster

Magnetoplasmadynamic (MPD) thruster is basically based on the principle of using the Lorenz force to generate thrust. The Lorenz force is a force in which an electrical charge moves in a direction perpendicular to a magnetic field. Plasma particles exist in an environment supplied with fields that are magnetic and electric. The magnetic field interacts with the current flowing in the plasma and is expelled by Lorenz forces and repulsion occurs.

1.2.5 Hall Effect Thruster

Hall thrusters create thrust by ionizing the propellant using an electric field instead of using the chemical fuel commonly used in rockets. Hall thrusters basically consist of a discharge channel, an anode and a cathode as shown in Figure 3. While voltage is applied, an electron movement occurs from the anode to the cathode. Electromagnets embedded in the pusher and moving in a circular motion create a magnetic field perpendicular to the electric field. This magnetic field stops the movement of electrons from the cathode to the anode along its circular motion and accelerates and ejects the gas particles. These particles, traveling outward at great speeds, create a backward thrust.

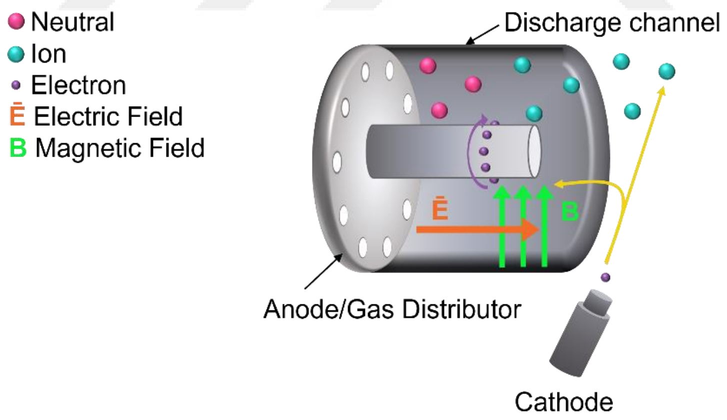

Figure 3. Working principle of a Hall thruster illustrating its key components

1.2.6 Gridded Ion Thruster

Ionized gas particles are moved by the electric field and pass through the grid structures. Each of these ion grid structures contains an aperture, which acts as a lens. Particles passing through the grid are focused at one point, creating thousands of ion jets. These ion jets create thrust.

1.2.7 Electrospray Thruster/Field Effect Electric Propulsion

When they are used in propulsion systems, electrosprey thrusters release thrust at low powers. Electrospray thrusters draw ions through apertures with the help of an emission. Commonly used Field Effect Electric Propulsion (FEEP) thrusters use liquid metals as the ion source and draw these ions through the emission to create thrust.

1.3. DBD Ion Thruster

Dielectic barrier discharge (DBD), as characterized in Figure 4, usually involves two electrodes, one exposed and one embedded, and a dielectric material placed between the electrodes

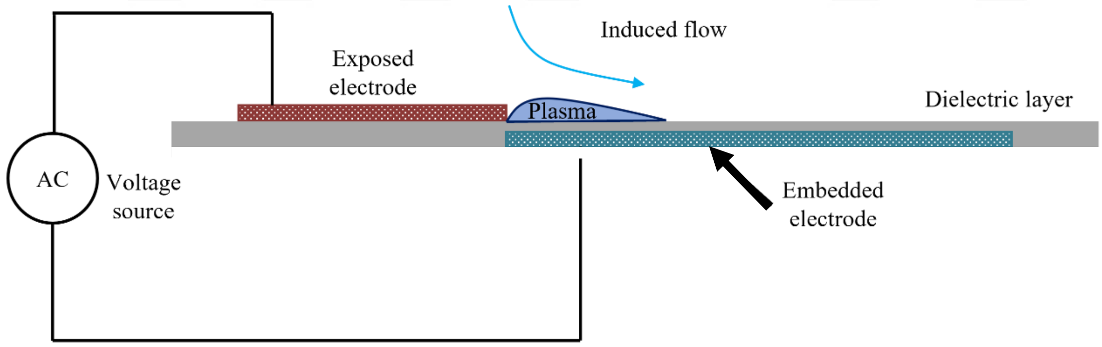

Figure 4. Schematic drawing of the DBD ion thruster

When high voltage is applied, the air passes through the zone formed on the exposed electrode, releasing ion winds to form the ion thruster. This ion thruster has many advantages such as its ability to operate without any moving mechanism, fast response time, low weight and uncomplicated structure, making it a potential alternative among propulsion devices. However, in order to improve its performance and prolong its lifetime, researchers have been working on ring-type ion thrusters, especially those used in space. In these studies, the geometrical properties, electrical properties and the material of the dielectric used are generally considered to improve the performance of ion thrusters.

1.3.1. Geometrical Parameters

Based on their geometric shape, ion repellants are broadly classified into two types: linear and annular. Ion thrusters in which the electrodes are placed linearly on the dielectric material are called linear ion thrusters. Especially in airplane wings, linear types are used to improve performance by reducing drag and increasing lift. Annular ion thrusters are formed by placing the electrodes in a circular shape. These structures are generally called as annular, but it can also have geometric shapes such as hexagonal or octagonal. It is known that annular structures are more preferred because they produce a annular flow structure in the field of jet flow for space field.

1.3.2. Electrical Parameters

In the thrust generation of DBD ion thrusters, many electrical parameters such as frequency value, signal type (sine, square etc.), applied voltage, duty cycle are examined. Generally, one of the parameters subject to studies is the frequency and voltage value, and as these two values are increased, the value of the thrust obtained increases. As a result of a series of experiments conducted by Borghi et al. (2008), it was revealed that both the momentum transfer and the thrust value increased with the increase in excitation frequency and applied voltage (Borghi et al., 2008).

1.3.3. Material Properties

One of the most important issues investigated to improve the performance of the ion thruster is the type of dielectric material. When producing DBD ion thrusters, Kapton is one of the most preferred materials in order to eliminate electrical conductivity. The thickness of the material has also been used the subject of research. VanDyken et al. (2004) stated that the lifecycle of a thicker kapton is longer, so that the voltage that can be applied to this ion thruster can be higher

(Van Dyken et al., 2004). In the literature, it has been observed that other materials such as polyamide-based nylon/PA2200 (Correale et al., 2015), silicone rubber, teflon (Roslı et al., 2022), quartz (Abdollahzadeh et al., 2014) can also be used as dielectric material.

2. LITERATURE REVIEW

2.1. Plasma Physics

Plasma, the fourth state of matter, is an ionized gas. When a solid is placed in a sufficiently hot environment, the crystals in it separate to form a liquid. When the liquid is heated, the unbound electrons and positively charged ions in it start to move freely. This movement creates a complexity as well as the release of great energy. This colliding molecular plasma is released (Bellan, 2008).

In the early 20th century, Irving Langmuir first used the word plasma to describe an ionized gas. In one of his studies, Langmuir examined the transport of electrons in the liquid in tungsten bulbs and observed the boundary layers formed between surfaces under the name of plasma sheath theory (Langmuir, 1919). In the 1940s, Hannes Alfvén developed the magnetohydrodynamic (MHD) theory, which studies the behavior of fluids when they enter a magnetic field. According to MHD theory, particles charged with certain charges can suddenly accelerate to high speeds and solar flares can occur due to the energy released (Bansal, 1994). With Alfvén's development of MHD, the use of this theory has become widespread in the formation of stars, solar winds and many other subjects such as solar flares. The interest in fusion energy, which started in the early 1950s, became more popular, especially among researchers, with the invention of the hydrogen bomb in 1952. In 1958, the field of plasma physics in space emerged with James A. Van Allen's discovery of the radiation belt that emerged as a result of the Earth's magnetic field and protected the Earth from the sun and other harmful rays (Li, 2019). With the introduction of plasma in lasers, the industrial market experienced a significant transformation. Since the 1960s, various propulsion systems that can be integrated into spacecraft have been developed using plasmas (Jahn et al., 2003). The use of ion thrusters, which are among these propulsion systems, has become quite widespread in both aviation and space in the last 20 years. Ion thrusters are generally divided into two classes; linear type and annular type. Linear type thrusters are mostly used in aircraft wings to increase lift and decrease drag in flow control, while annular type thrusters are used for thrust generation in spacecraft due to their annular jet characteristics.

2.2. Linear Type Ion Thrusters

Borghi et al. (2008) investigated the effect of electrohydrodynamic (EHD) on momentum transfer using direct current (DC) voltages with different phases and what is effective in controlling the boundary layer. The experimental results show that the efficiency of EHD increases when more than one phase power supply is used, and the momentum transfer increases when the voltage and frequency are fed at high values. In addition, experiments conducted in the wind tunnel, increasing the flow velocity decreased the electrohydrodynamic effect and momentum transfer (Borghi et al., 2008). In another study, Borghi et al. (2017) investigated the stall condition recovery of an array of deployed electrodes with on/off frequency cycling and jet generation at different angles on the NACA0015 blade. As a result of the experiments, it was observed that the highest effect of the DBD plasma actuator on stall recovery was observed at the leading edge placement of the wing, i.e. the actuator pairs shown in Figure 5. No significant result was observed for the jet with different cycles. Also, a function between the free flow velocity and on-off cycle frequency was found (Borghi et al., 2017).

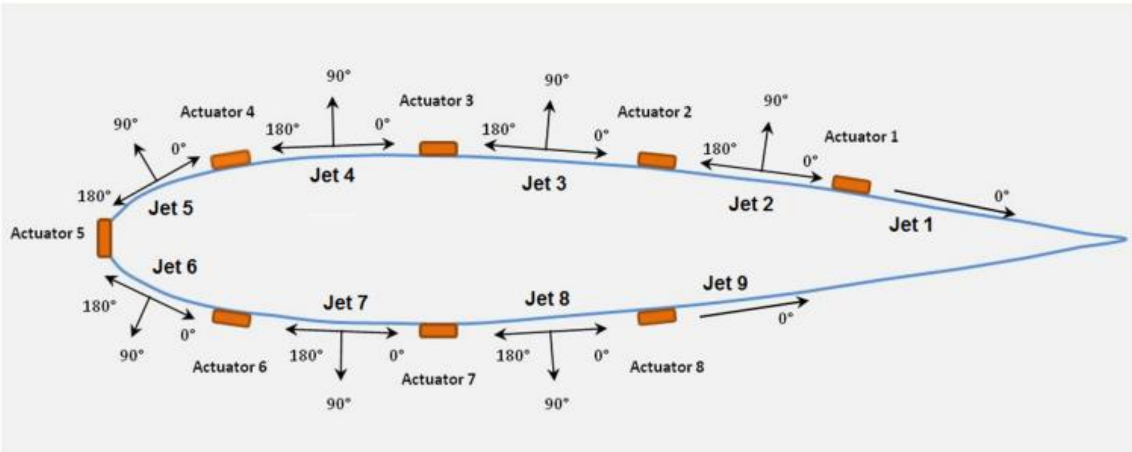

Figure 5. Arrangement of electrode pairs on the NACA0015 wing (Borghi et al., 2017)

Cristofolini et al. (2012) conducted a series of experiments to observe the momentum transfer process. Different AC currents were applied to a DBD ion thruster with Teflon dielectric material placed between two electrodes. The velocity distribution of the impulse generated by the wall jet and the vortex morphology were visualized at all given currents. As it can be seen in Figure 6, the vortex formation was visualized for four different condition using the Schlieren technique.

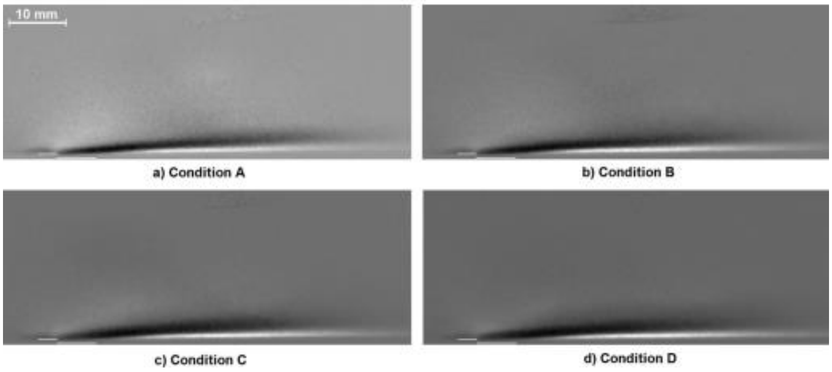

Figure 6. Schlieren visualization of generated vortexes by the actuator in continuous regime (Cristofolini et al., 2012)

In order to get a deeper understanding of the EHD effect in steady state, velocity profiles were generated using the pitot technique and this profile was compared with the Schlieren visualization technique. The graph for pitot technique is shown in Figure 7. This graph shows the region under EHD interaction approximately 7 mm above the actuator surface (Cristofolini et al., 2012).

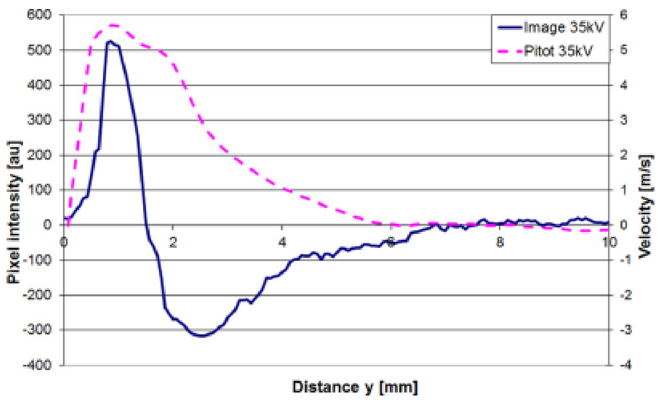

Figure 7. At 35 kV, velocity profiles and pixel intensity generated using Pitot and Schlieren imaging techniques (Cristofolini et al., 2012)

Hoskinson et al. (2008) measured the thrust of two different DBD ion thrusters, single and double layer. Two types of electrode geometries, linear and annular, were used in both actuators. Figure 8 shows the actuator arrays.

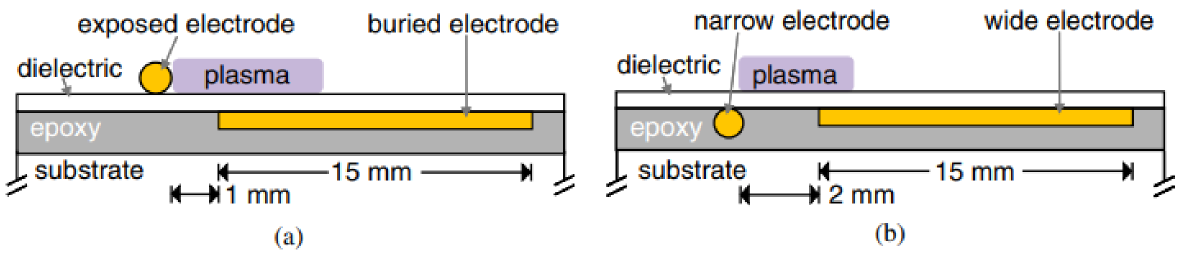

Figure 8. Schematic of a) single barrier dielektric discharge and b) double barrier discharge (Hoskinson et al., 2008)

As a result of increasing the applied voltage to the double-layer ion thruster, it was observed that the thrust values were higher in actuators where the diameter of the electrode was small. In single-layer actuators, this enhancement is exponential rather than linear.

The changes in the velocity profile are shown in Figure 9. In the single dielectric barrier discharge actuator, relatively small differences were observed in all 4 variables, while in the double barrier disharge, the peak velocity increased by 50% after 90 minutes of operation (Hoskinson et al., 2008).

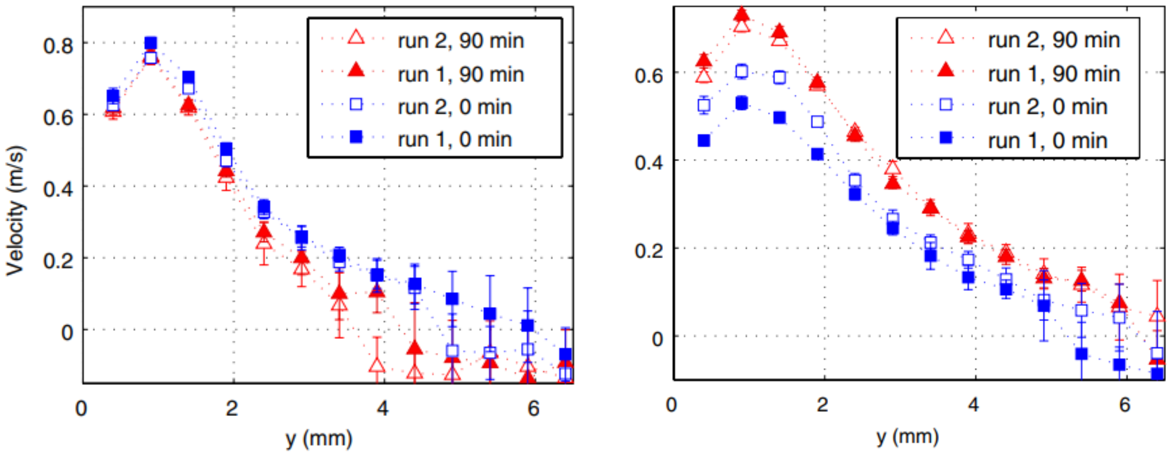

Figure 9. Velocity profiles of single barrier and double barrier discharge (Hoskinson et al., (2008)

Shin and Raja (2007) previously conducted a similar study in a parallel plate actuator. They observed recurrent variations of the discharge and emphasized that the shift occurred due to the secondary electrode changing the emission coefficient (Shin et al., 2007).

Komuro et al. (2017) tested the gas changes near the thrust generated by a ns-dielectric barrier discharge plasma actuator (nanosecond-DBDPA). The ns-DBDPA actuator generates a pressure wave and the gas produces stochastic irregularities near the leading edge of the wing.

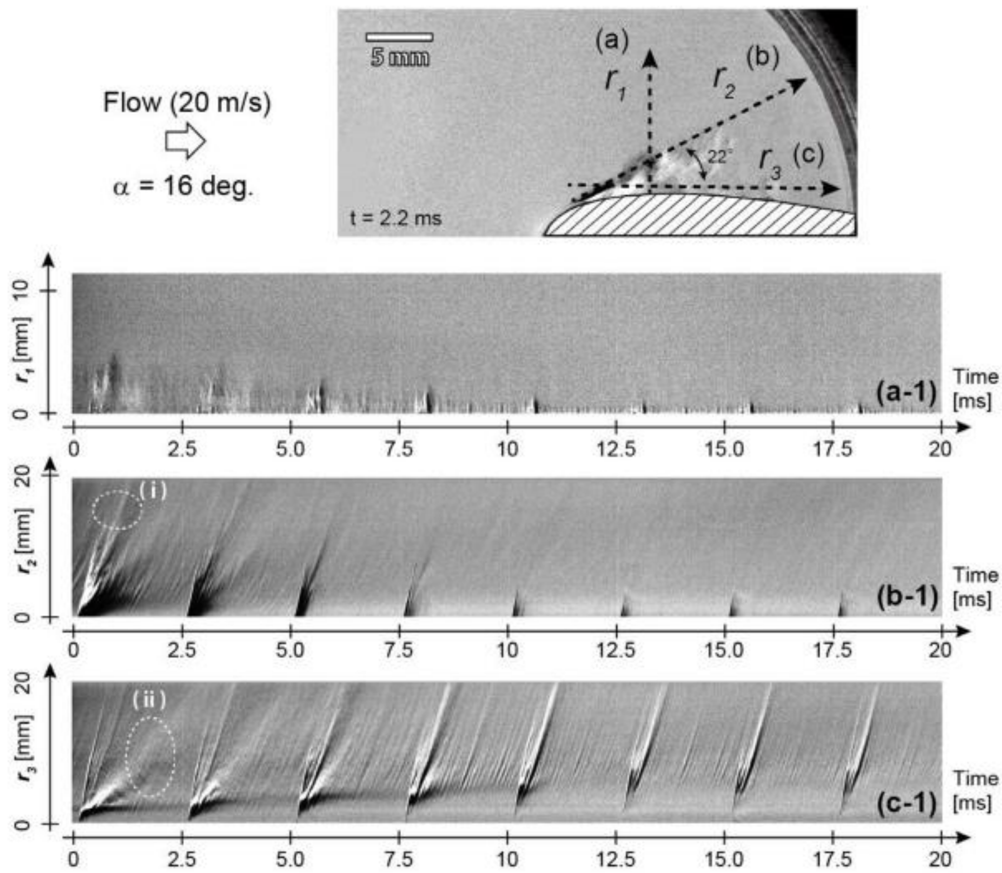

Figure 10. Gas densities imaged with α=16° Schlieren imaging technique (Komuro et al., 2017)

Figure 10 shows that the first pulse discharge produces a heated gas and this heated gas spreads towards the trailing edge of the blade. As it can be seen in the Figure 10, the diameter of the gas increases gradually and its density decreases. At this point, Komuro proposed that the ns-DBDPA actuator recovers a negative C_p value at the leading edge of the blade (Komuro et al., 2017).

Thomas et al. (2009) tried to optimize and to improve the thrust generated by the actuator with increasing the Reynolds number for flow control. Many parameters such as dielectric material, dielectric thickness, electrode geometry, electrode array, applied voltage, excitation frequency and even signal type were analyzed.

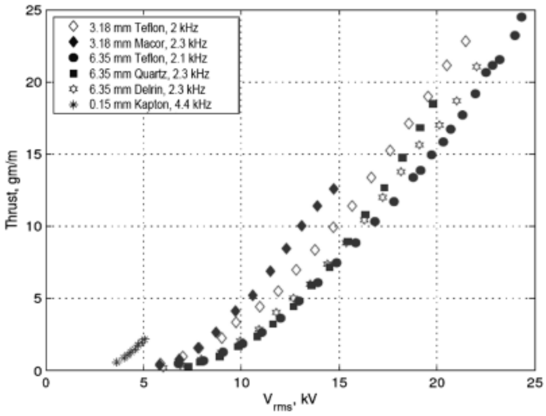

Figure 11. Thrust measurement for different dielectric materials and thicknesses (Thomas et al., 2009)

It is clear from Figure 11 that teflon dielectric based plasma actuator has the highest thrust value among all materials, with a thickness of 6.35 mm and a frequency of 2.1 kHz. The thrust value obtained in the experiment using a thicker teflon is higher than that of kapton. It is also seen that as the thickness of the dielectric material increases, the dielectric plasma actuator can withstand much higher voltage values.

In another stage of the study, Thomas et al. (2009) analyzed the frequency parameter and plotted the graph shown in Figure 12.

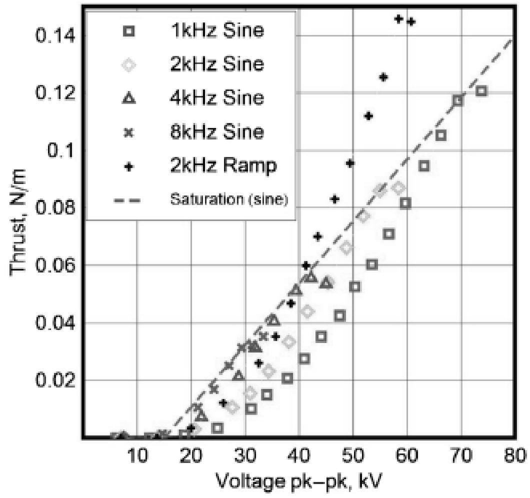

Figure 12. Thrust values according to applied voltage at different frequencies (Thomas et al., 2009)

The graph shows the effects of AC frequency on thrust-voltage changes. In the experiments a sinusoidal waveform was used as it is generally able to overcome the disturbances caused by inductance. It is clear from Figure 7 that the saturation of the thrust value increases with enhancement of frequency as AC frequency decreases. This increment in voltage shows a linear variation. Thomas et al., 2009 mentioned that the various parameters studied in this study is that using an electrode with a threaded edge produces more thrust than ion thrusters using a conventional flat electrode (Thomas et al., 2009).

In a study published by Asphis et al. (2014), the thrust force generated by DBD plasma actuators with different excitation frequency and applied voltage values are investigated. In their experimental results, it is observed that negative thrust or "anti-thrust" values at low frequencies between 4 Hz and 64 Hz were found.

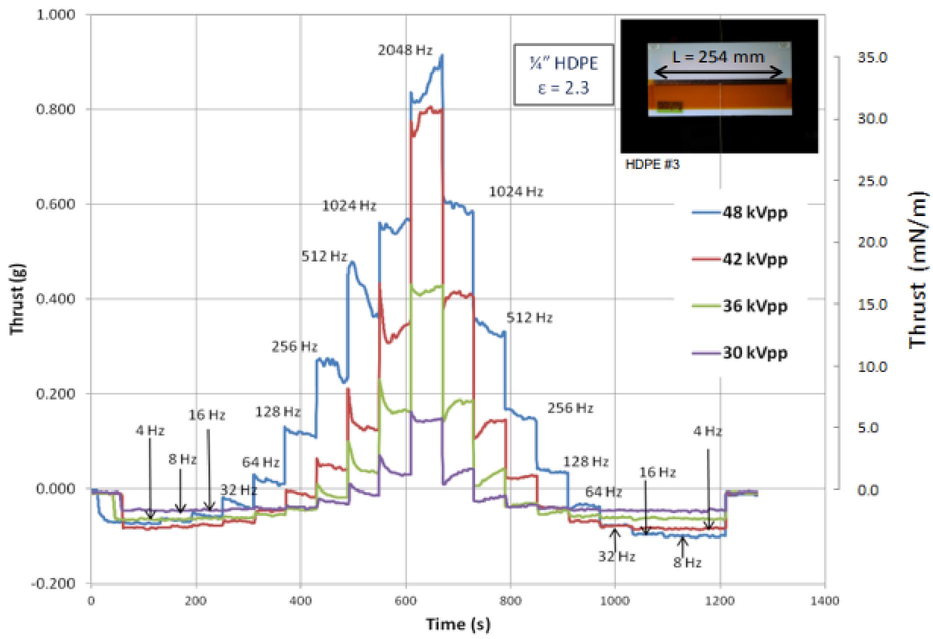

Figure 13. Frequency values at constant voltage (Asphis et al., 2014)

Copper tape electrode with a length of 254 mm was used in this study. In addition, High Density Polyethylene (HDPE) dielectric material with dielectric constant (ε) 2.3 was used in the production of DBD plasma actuator. When the data in Figure 13 is analyzed, asymmetry and hysteresis were found even at a constant 48 kV_{pp} value. Asphis (2014) concluded that the descending data line in the graph is more reliable in this study because the scans at the descending frequency are more consistent.

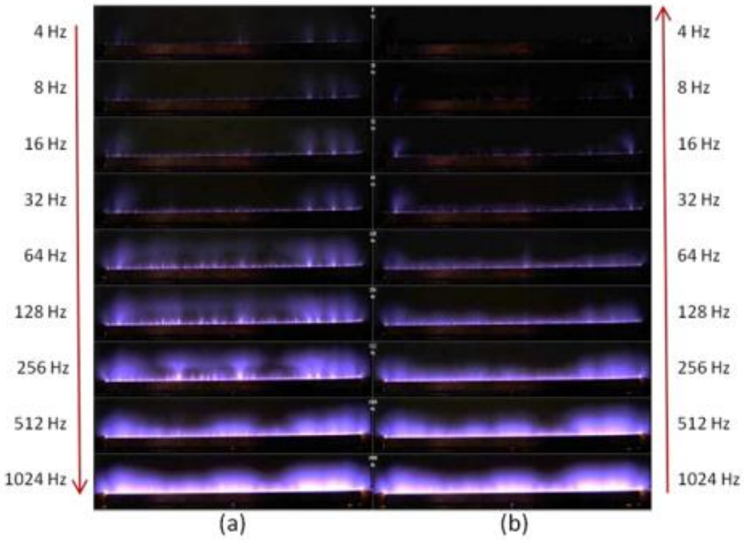

Figure 14. Frequency dependent plasma discharge views (Asphis et al., 2014)

In addition, plasma images were taken depending on the frequency change, as shown in Figure 14. It was observed that the higher the frequency, the higher the height of the ion winds formed and the more intense ion winds are (Ashpis et al., 2014).

Vernet et al. (2015) investigated the flow around a circular cylinder immersed in a flat plate for flow control. In the experimental process, they placed a double-sided DBD plasma actuator in the cylinder and aimed to find the best position that can be achieved by changing the position of this actuator. As a result of the experiment, they optimized the position of the DBD plasma actuator and reduced the friction by 30%. A visualization of the experimental setup is shown in Figure 15 (Vernet et al., 2015).

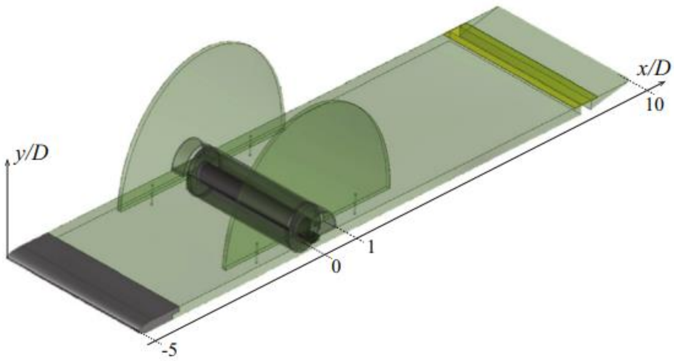

Figure 15. Visualization of the experimental setup (Vernet et al., 2015)

Akbıyık et al. (2017) placed linear and partial plasma actuators on the airfoil with certain parameters. In their study, two SDBD plasma actuators with different configurations and one linear plasma actuator were used. They stated that the linear plasma actuator exhibits a 2D flow, while the geometrically modified SDBD plasma actuator transforms the flow around the wing from 2D to 3D.

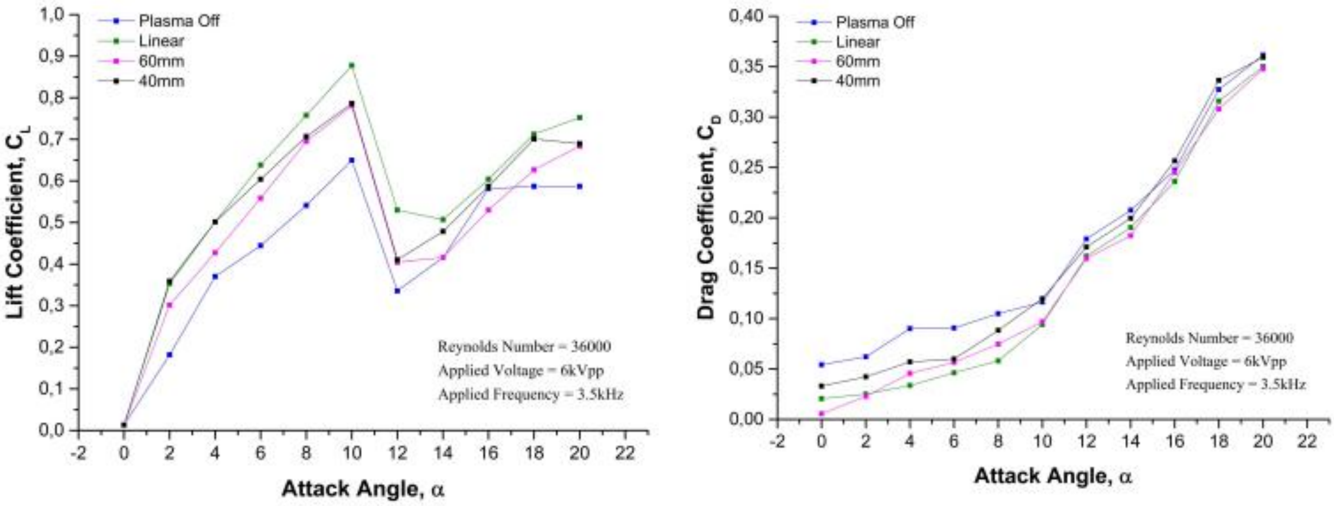

Figure 16. Lift and drag coefficients by increasing angle of attack (Akbıyık et al., 2017)

Figure 14 shows the variations of drag and lifting coefficients at certain Reynolds number, applied voltage and excitation frequency depending on the angle of attack. When the graph is examined, stall occurs when the angle of attack is 10̊. By changing the number and position of the plasma actuators, the stall angle can be shifted to a reasonable level. In this study, these strong effects with plasma actuators are reduced the drag coefficient. It has been reported that the maximum reduction in drag is observed between attack angle of 4º and 10º (Akbıyık et al., 2017).

Riherd and Roy (2013) investigated the effect of two different DBD ion thruster geometry. In one of the geometry they used as active flow control technique, they investigated how the traces of a boundary layer at zero pressure gradient are formed. Secondly, they simulated the flow at low Reynolds numbers by accelerating the flow and making it more powerful. In their study, they showed that using a plasma actuator with serpentine geometry improves efficiency by combining various flow control methods. The geometries are shown in Figure 14. The main principle they addressed was that different actuator geometries, are flow control device, are required because aircrafts need specific lift forces (Riherd et al., 2013).

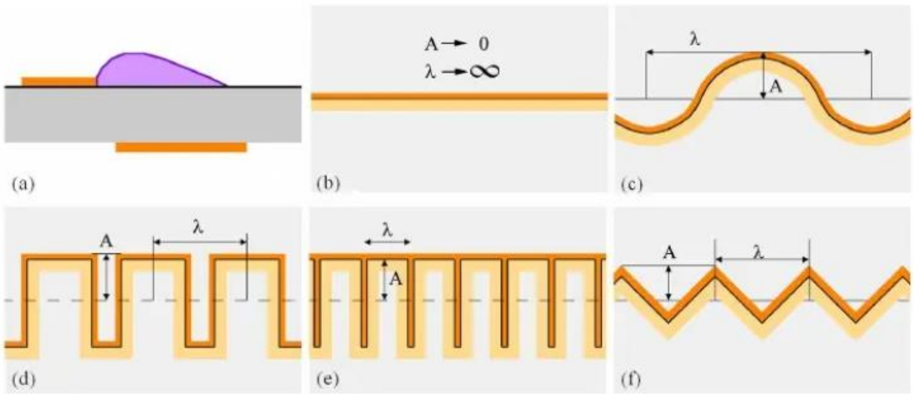

Figure 17. a) Schematic of DBD, b) lineer, c) arc, d) rectangle , e) comb, f) triangle serpentine actuators (Riherd and Roy, 2013)

2.3. Annular Type Ion Thrusters

Annular type ion thrusters are an improved version of the traditional linear type ion thruster to provide a better ion flow and to produce a more efficient thrust. In this type of the ion thruster, the ions are accelerated in a ring shape, providing better control to create a better targeted thrust. Furthermore, annular type ion thrusters can offer advantages such as lower energy consumption and longer operating life. Therefore, annular type ion thrusters are widely used in space applications such as spacecraft and satellites.

According to the results reported by Zhou et al. (2022), thrust increases with increasing power when the pressure remains constant. The study focused on the point between the values where the atmospheric pressure is low and the altitude is close to space. The exposed electrode is made of stainless steel copper material and the embedded electrode is made of kapton-coated copper foil. The quartz glass body was used as a dielectric material to prevent electrical discharge between the two electrodes. The structure of the DBD ion thruster is shown in Figure 18.

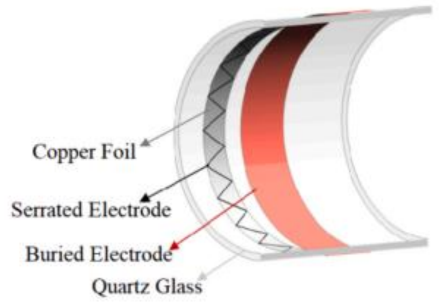

Figure 18. Structure of the DBD ion thruster (Zhou et al., 2022)

As a result of their experiments, the power change depending on air velocity is given in the graph in Figure 19. At constant air pressure, the power increases as the air velocity increases. The most important point here is that the air velocity reached its maximum value at 870 Pa and 1.6 kPa, and the air velocity decreased with increasing power (Zhou et al., 2022).

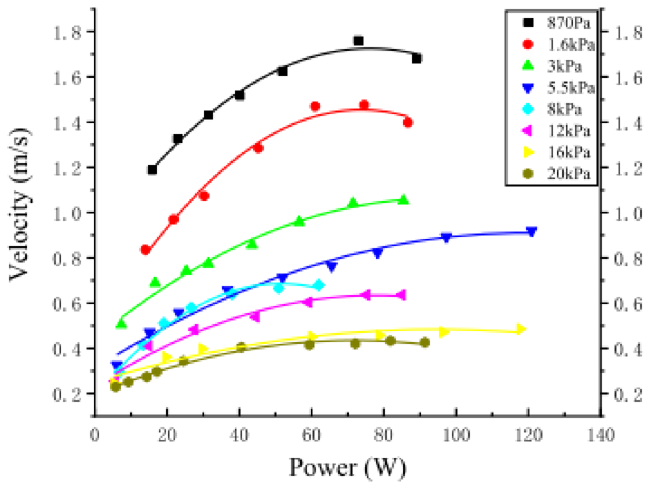

Figure 19. The relationship between velocity and power (Zhou et al., 2022)

Chabert et al. (2012) injected neutral propellant Xe gas into the case at a constant rate and generated a plasma by circulating a RF current in the coil. The ions produced in the plasma were accelerated and the Xenon atoms flowed from the propellant through the gratings. Based on the particle and energy balance equations, they discussed four variables: plasma density, electron temperature, atomic density and atomic temperature.

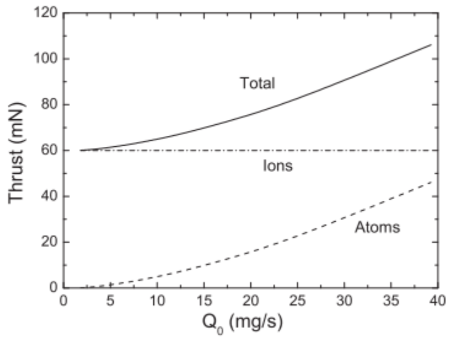

Figure 20. Thrust values generated by atoms and ions (Chabert et al., 2012)

As shown in Figure 20, the contribution of atoms to the thrust increases with time. In this high regime, the thruster operates at low specific thrust and very low MUE. In terms of mass utilization efficiency, it is better to operate at low gas flow rate. The results show that the MUE decreases rapidly with the gas flow rate and the RF power transfer efficiency increases significantly with the injected gas (Chabert et al., 2012).

A study by Craig et al. (2011) investigates the flow field structure of an annular DBD plasma actuator. These actuators are investigated for use as spanwise-periodic discrete roughness elements on sweep vanes for laminar flow control. In the study, holes with diameters ranging from 3 mm to 7 mm are considered. In addition, an array of five 3 mm diameter actuators is also investigated. A schematic view of the plasma actuators investigated is presented in Figure 21. It is shown that the flow field structure is sensitive considering the hole size and the applied voltage. For the array actuator, the vortices are greatly constricted as a result of interaction from neighboring holes. This study is a first step towards understanding the physical mechanisms of plasma actuators for laminar flow control in swept vanes (Craig et al., 2011).

Humble et al. (2013) investigated the spatio-temporal structure of a millimeter ring type DBD plasma actuator. According to the data obtained from their results, the plasma was able to maintain a regular spatio-temporal structure after discharge. They also found that plasma actuators are not only effective in controlling flow but also promising in controlling flow disturbances as they pass through the turbulence boundary layer.

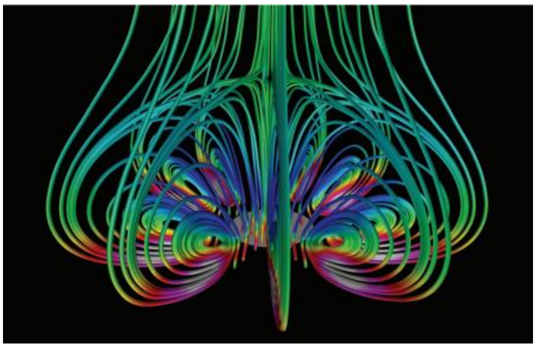

Figure 21. Visualization of vortex images generated by plasma actuators with PIV method (Humble et al., 2013)

When the plasma actuator is operated in a quiescent flow field, as shown in Figure 21, it creates opposing vortices as well as a 3D toroidal jet region. However, contrary to popular belief, these vortices move in the opposite direction to the vortices created by annular designs, creating a velocity field. Humble mentioned that this flow may be due to the millimeter scale and positions the actuators closer together. In this way, the vortices created by each actuator merge with the vortices of neighboring actuators and the vortex size is significantly reduced (Humble et al., 2013).

Neretti et al. (2017) investigated DBD plasma actuators with linear and annular structures. For the electrodes with a ring structure, electrodes of different diameters were tested, while for the linear type electrodes, the distances of the electrode were tested. Figure 22 shows the electrode structures schematically.

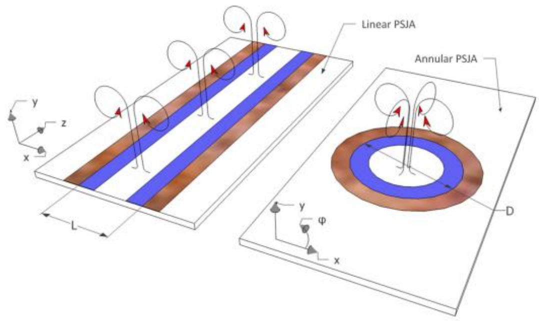

Figure 22. Schematic view of geometries: linear (left) and annular (right) (Neretti et al., 2017)

The electric power versus distance and diameter of the electrodes are defined in Figure 23. The blue line is applied to the linear actuator and the red line to the annular actuator. The electric power increases as the distances of the electrodes increase in the linear actuator up to a certain range and then decreases. However, in the annular actuator, the electric power increases as the diameter of the electrode increases (Neretti et al., 2017).

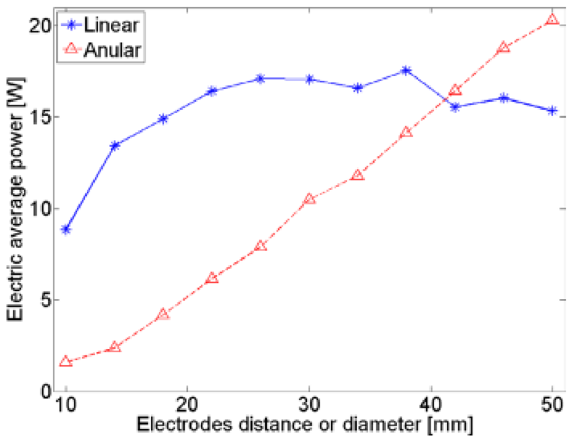

Figure 23. Electric power versus electrodes distance and diameter (Neretti et al., 2017)

In this study, the annular electrode geometry found in the literature and the sinus geometry, which is different from the structures in the literature, were examined. When the studies in the literature are examined, the most similar study to this study is the study published by Neretti et al. (2018) in which annular and octaganal geometries are examined (Neretti, 2018). The geometry used as annular shapes with diameters of 5 mm, 10 mm, 15 mm and 20 mm. Considering the axisymmetry, measurements were made by changing the amplitude for each ring. Kapton was used as the dielectric material and this kapton was placed in different numbers for each experiment. For each geometry, experiments were conducted with 1 layer, 2 layers and

3 layers of kapton and thrust values were obtained. Due to the annular and symmetrical structure of the sinusodial annular ion thruster, it is aimed to obtain much higher thrust compared to standard models by starting the flow from different points on the circle. In addition, the ring structure of the geometry chosen in this study is thought to provide a higher thrust by integrating into the ion engines used in space studies.

3. MATERIALS AND METHODS

3.1. Experimental Setup

In aerospace field, S-DBD plasma ion thrusters have become very popular in recent years due to their ability to generate electrical impulse by interacting with air pressure in the flow control field. An ion thruster usually consists of a pair electrodes, one electrode is embedded and the other one is exposed. The dielectric material is placed between them. When the HV is applied to the exposed electrode, an ion wind occurs and it generate the thrust. This ion thruster can be used as an alternative option among propulsion devices due to its many advantages such as its ability to operate without any moving mechanism, fast response time, low weight and uncomplicated structure. In this study, DBD plasma actuators with annular and sinusoidal geometry were used to improve the performance of ion thrusters. Neretti et al. (2018) examined geometries with annular and octaganal structures (Neretti., 2018).

3.1.1 Generation of Ring Plasma Actuators and Parameters to be Analyzed

The plasma actuator which is used in this thesis study was selected to be in annular and sinusoidal form. Figure 24 shows the annular and sinusoidal actuator configuration drawn using the SolidWorks program.

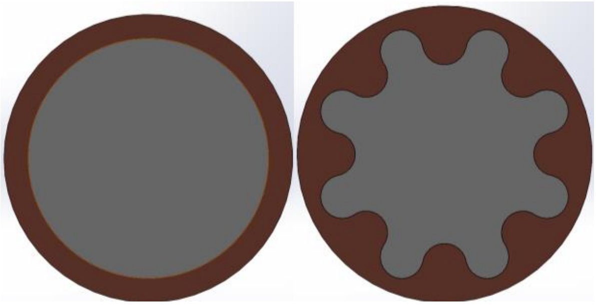

Figure 24. CAD drawing of an annular and sinusoidal plasma actuator

The geometry is arranged as axisymmetric and the circle diameters is chosen as 5 mm, 10 mm, 15 mm, and 20 mm. Two different amplitudes are varied for the sinusoidal geometry at each diameter. For each geometry, the thrust values are measured considering the different layer numbers of the Kapton. The number of the layer is chosen as 1 layer, 2 layers and 3 layers. For each geometry diameter, the frequency was kept constant at 3.5 kHz and thrust measurements were made by varying the given voltage values. The research parameters for the thrust improvement are investigated. These parameters are given in Table 1.

Table 1. Parameters to be examined.

No	Parameter	Definition	Values to investigate		
1	D (mm)	Annular diameter	5	10	15
2	d (mm)	Radius of one side of the sinusoidal geometry	0.5, 1	1, 2	1.25, 2.5
4	Layer(s)	Kapton Dielectric Material	1, 2, 3	1, 2, 3	1, 2, 3
5	V (kV_{pp})	Applied voltage		4, 6, 8	
6	f (kHz)	Excitation frequency		3.5	
7	Dielectric Materail Types	Dielectric Materials		Plexiglass, Carbonfiber, Fiberglass, Kapton	
8	t (mm)	Dielectric Materials Thickness		0,6 , 0,9	

Considering the axial symmetry of the sinusoidal DBD plasma actuator, different amplitudes were determined for each inner diameter value as seen in Figure 25. These amplitudes were determined as 0.5 and 1 mm for 5 mm, 1 and 2 mm for 10 mm, 1.25 and 2.25 mm for 15 mm. All electrodes are produced based on these parameters.

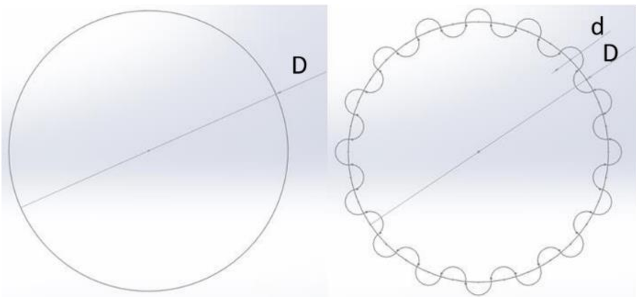

Figure 25. Base model and sinusoidal geometry at D diameter

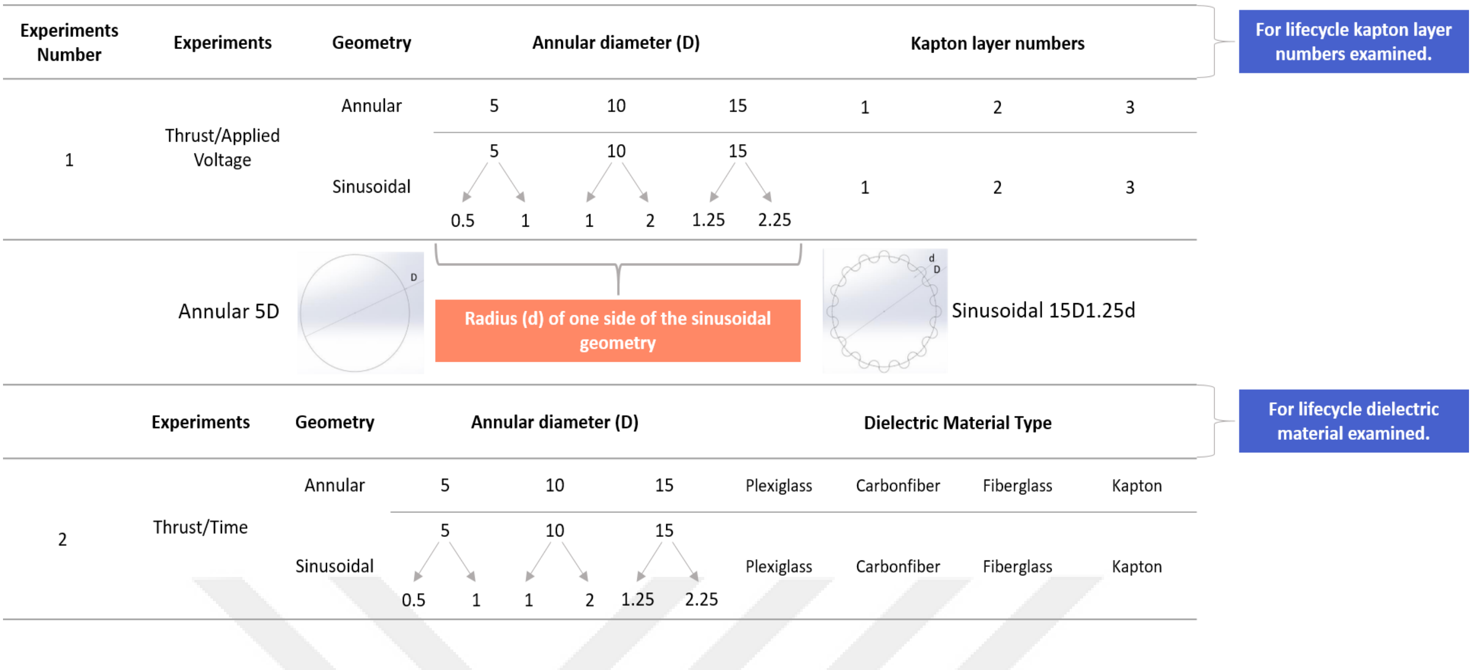

Figure 26. The diagram of the experiments

The electric and magnetic fields will affect the DBD plasma actuators in the annular structure and material lifecycles. For these reasons, the material of the electrodes of the DBD plasma actuators are chosen as copper. The dielectric material is chosen as the Kapton and placed between the these two electrodes. The layer number is obtained as 3 different layers of Kapton. These layers are 1 layer, 2 layers and 3 layers as shown in Table 1. For the DBD ion thruster production, 4 different types of dielectric materials were selected as seen in Figure 26. These dielectric materials are chosen as plexiglass, carbonfiber, fiberglass and kapton.

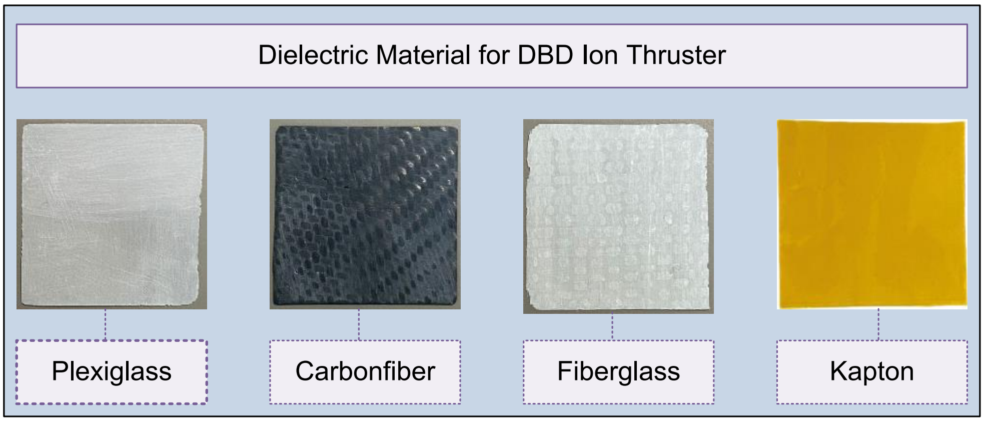

Figure 27. Dielectric material for DBD ion thruster

All these steps for the production of dielectric materials are shown in the flow chart in Figure 27. Firstly, the raw material is selected. Secondly, the mixture was obtained by using hardener and epoxy resin raw material in certain ratios. In the 3rd process, wax was applied on a hard and flat surface to prevent the composite materials from sticking to the surface. Glassfiber and carbonfiber material is laid on the surface. Epoxy resin raw material is applied to the glass fiber and carbon fiber laid on the surface. After a certain period of time, the hardened composite material is cut with the Dremel device. The composite materials cut according to the determined parameters are brought to the desired thickness with the help of sanding process and the production of DBD ion thrusters with different types of materials is completed.

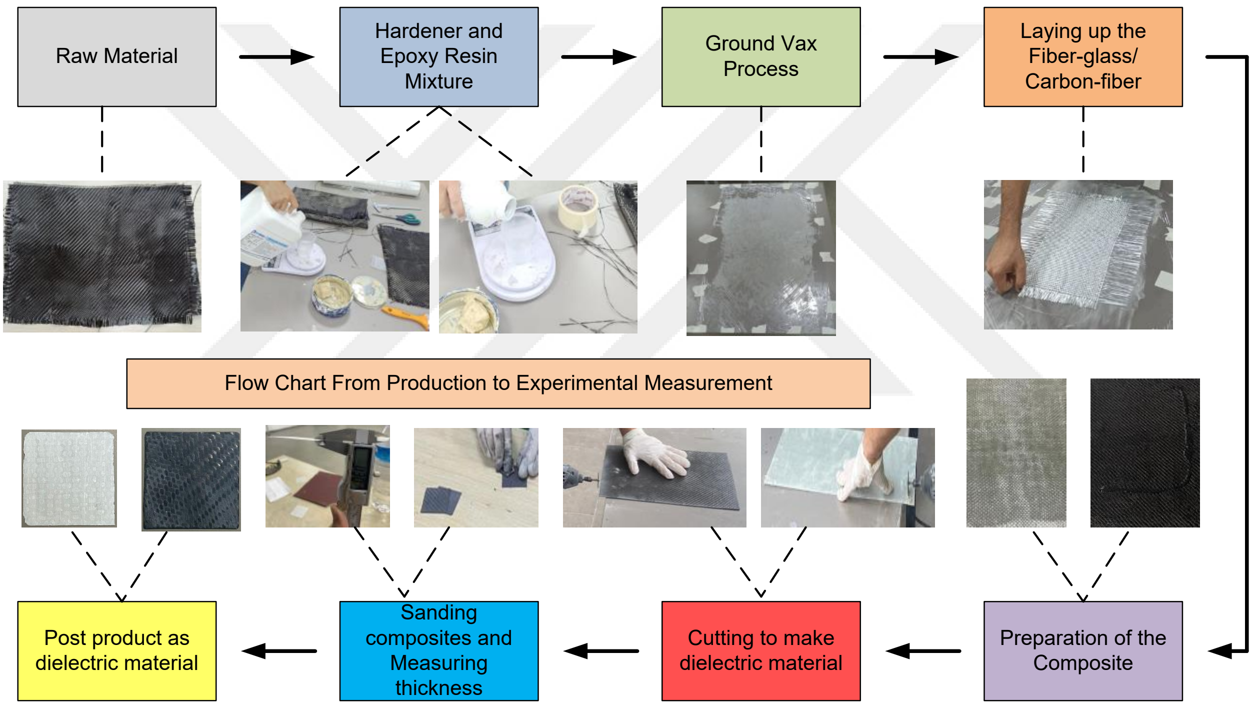

Figure 28. Flow chart from production to post-product

In order to produce the DBD plasma actuator, the dielectric material is selected and the embedded electrode is first placed on the bottom and covered with dielectric material. Exposed electrode is placed on the dielectric material. After the electrode connections for the voltage probe and current probe are made, the production of the DBD plasma actuator is completed. The visualization of the fabricated DBD ion thruster with sinusoidal geometry is given in Figure 28.

Figure 29. Completed production of DBD ion thruster

3.1.2 Experimental Setup of the Plasma Generation

The connections of the DBD ion thruster system, annular plasma actuator electrode structure, and equipments for plasma generation are illustrated in Figure 29. An adjustable high-voltage amplifier are used with an applied voltage from 4 kV_{pp} to 8 kV_{pp} and a variable kapton layer ranging from 1 layer to 3 layer. P6015A model high voltage probe are connected to the embedded electrode, while the other will be connected to the exposed electrode. The current and voltage from the high-voltage amplifier are controlled using voltage and current probes, and the changes in electrical voltage with time are observed using an TDS2020C model oscilloscope. This setup allows for easy adjustment of the applied voltage and excitation frequency.

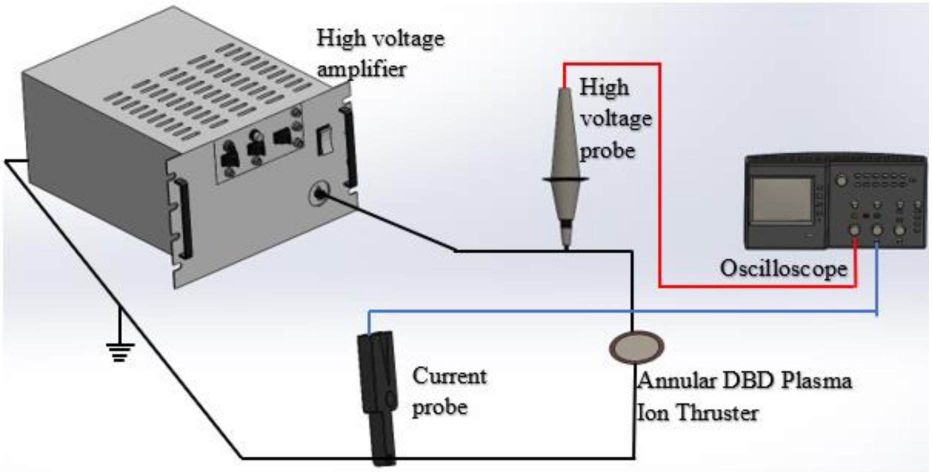

Figure 30. The schematic diagram of the ion thruster system and electrical equipment setup

With the discharge of the DBD ion thruster, thrust measurements were made by driving different applied voltage values in different geometries and diameters. The electronic thrust measurement device was used to measure the thrust generated by the DBD plasma actuator. The schematic view of this device is given in Figure 30.

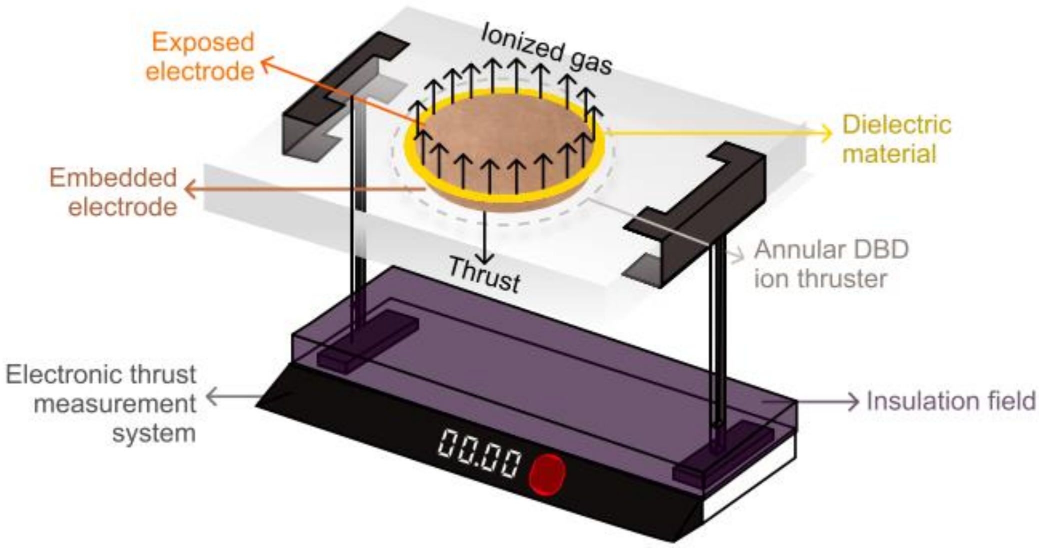

Figure 31. Schematic view of an electronic thrust measurement device

In order to protect the electronic thrust measurement device from being affected by electric field, it has been proposed to cover it with a protective case for safety. In the study by Hoskinson et al. (2008), a similar system was used to protect the DBD plasma actuator from electricity during discharge (Hoskinson et al., 2008). Similarly, McGowan et al. (2016) used an electronic thrust generation device to measure the thrust values produced by the pulsed DC plasma actuator and coated it to prevent the electric field (McGowan et al., 2016). Considering the studies in the literature, it was deemed appropriate to use an thrust measurement device in the experimental setup with a cover. In order to put the produced plasma actuators on this device, two support rods were designed by using a 3D printer as seen in Figure 31 and Figure 32. In this way, it will be possible to avoid any possible electrical contact of the device to be used in the measurement of thrust values.

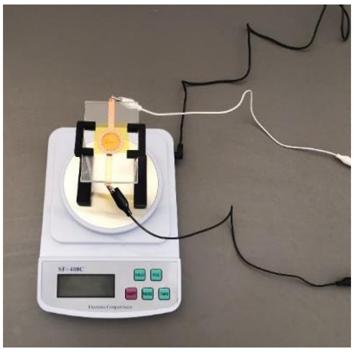

Figure 32. Experimental setup of an electronic thrust measurement device

Figure 33. Experimental setup of ion thruster system

4. RESULTS AND DISCUSSIONS

In this study, thrust performance in DBD ion thrusters is investigated in two stages. In the first part, the electrode geometry is changed from the annular model found in the literature, and the number of layers of the special sinusoidal model is changed. The thrust values generated by these models during the production of the plasma at different voltage values are presented. In the second stage, the time-dependent deformations of the DBD ion thrusters structures are shown.

4.1. The Effect of Different Layer Number and Size

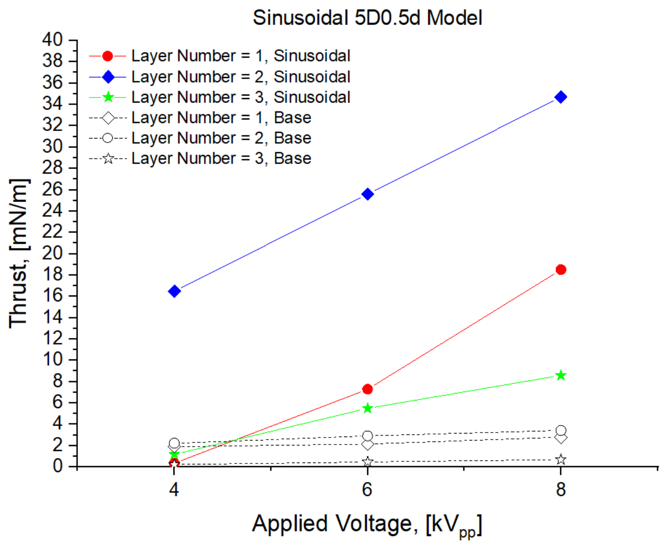

Figure 34. Thrust values of the 5D0.5d sinusoidal and annular geometry with different of number of layers

The graph in Figure 34 shows the thrust values depending on the voltage applied to the geometries of sinusoidal and annular models with diameters of 5D0.5d and DBD ion thrusters. For these models, the dielectric material is chosen as Kapton and the number of layers varies as 1 layer, 2 layers and 3 layers. When the graph is analyzed, the highest thrust value is seen in the sinusoidal 2-layer model with a diameter of 5D0.5d. Its thrust value increases when the applied voltage is increased and its value is 34.7 mN/m.

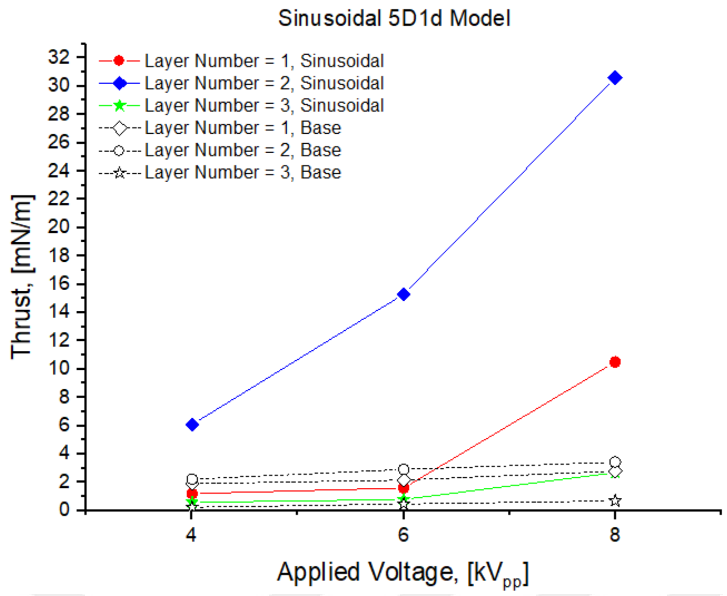

Figure 35. Thrust values of the 5D1d sinusoidal and annular geometry with different of number of layers

In the graph in Figure 35, 4 kV_{pp}, 6 kV_{pp} and 8 kV_{pp} voltage applied plasma actuator thrust values for the sinusoidal 5D1d diameter are presented. When the graph is analyzed, the highest thrust value was observed as 30.6 mN/m at 8 kV_{pp}. Compared to Figure 34, the thrust value decreases as the amplitude increases. One of the primary causes of this is that greater thrust is produced at smaller amplitudes, which is connected in a particular way and increases the ion collision forces in a smaller region.

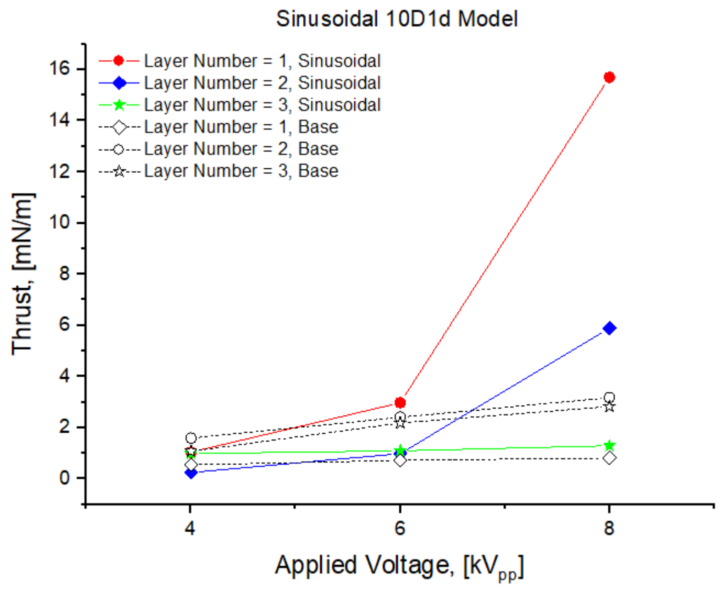

Figure 36. Thrust values of the 10D1d sinusoidal and annular geometry with different of number of layers

Figure 36 shows the thrust values depending on the applied voltage to the DBD ion thrusters with sinusoidal and annular 10D1d diameters. The voltages are applied as 4 kV_{pp}, 6 kV_{pp}, 8 kV_{pp} for different number of layers as 1 layer, 2 layers and 3 layers of kapton. When the graph is examined, it is seen that the highest thrust value is in the single-layer sinusoidal 10D1d model. The single-layer sinusoidal 10D1d model thrust value is about 1.05 mN/m and 2.98 mN/m at 4 kV_{pp} and 6 kV_{pp}, respectively. Then, the thrust value has a sudden increase which is about 15.7 mN/m when applied voltage is increased to 8 kV_{pp}. The main reason for this is that the effectiveness of the thrust value increases as the voltage is increased.

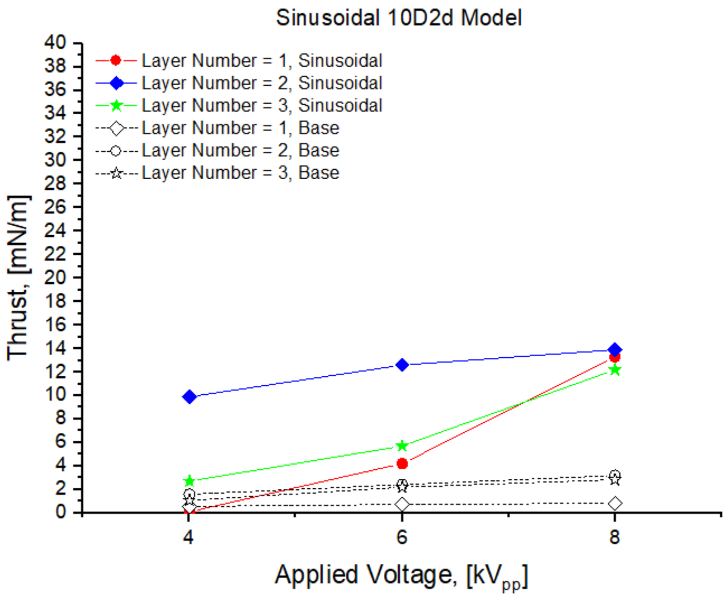

Figure 37. Thrust values of the 10D2d sinusoidal and annular geometry with different of number of layers

Figure 37 shows the thrust values of the DBD ion thrusters at 4 kV_{pp}, 6 kV_{pp}, 8 kV_{pp} for the sinusoidal and base models with a diameter of 10D2d for different layer numbers of Kapton. It is seen that the highest thrust value is obtained in the 2-layer sinusoidal 10D2d model at 8kV_{pp}. This thrust values is about 13.9 mN/m.

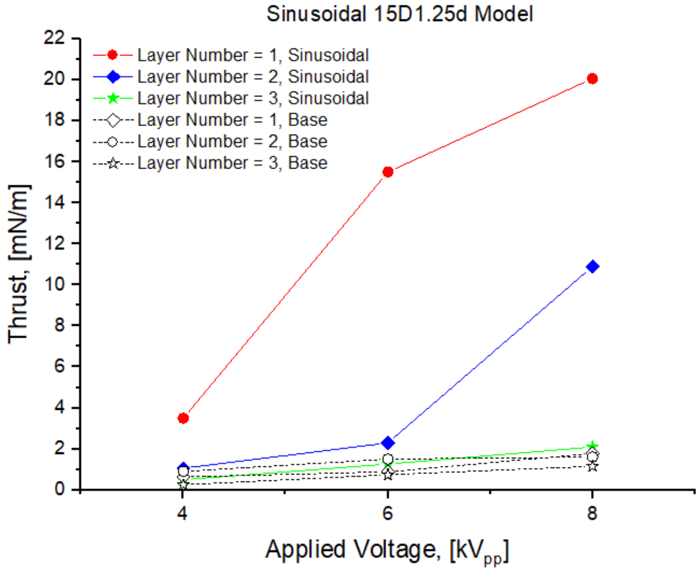

Figure 38. Thrust values of the 15D1.25d sinusoidal and annular geometry with different of number of layers

The graph in Figure 38 shows the applied voltage dependent thrust values of the DBD ion thrusters with sinusoidal and annular 15D1.25d diameters with 1 layer, 2 layers and 3 layers of kapton. When the graph is examined, it is seen that the highest thrust value is about 3.5 mN/m in the single-layer sinusoidal 15D1.25d model at 4 kV_{pp}. The highest thrust values are about 20.05 mN/m in the 2-layer sinusoidal 15D1.25d model.

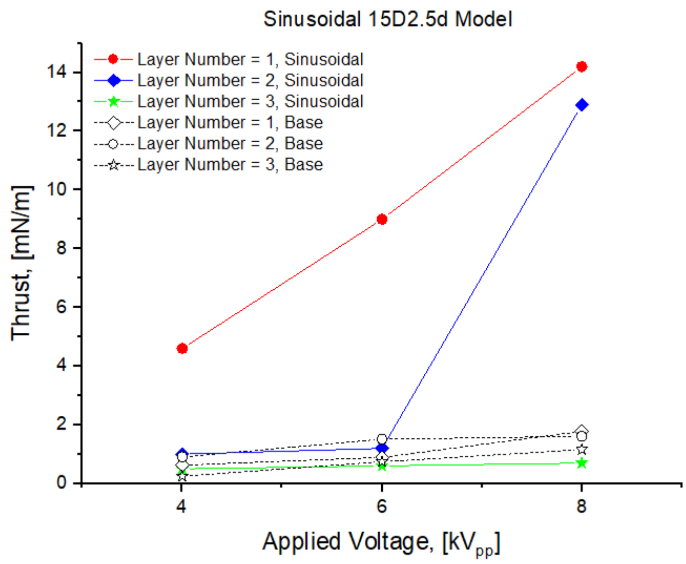

Figure 39. Thrust values of the 15D2.5d sinusoidal and annular geometry with different of number of layers

The graph in Figure 39 shows the applied voltage dependent thrust values of the DBD ion thrusters with sinusoidal and annular 15D2.25d diameters with 1 layer, 2 layers and 3 layers of kapton. When the graph is examined, it is seen that at 8 kV_{pp}, there two high thrust value which are taken from 1 layer and 2 layer dielectric material based ion thruster.

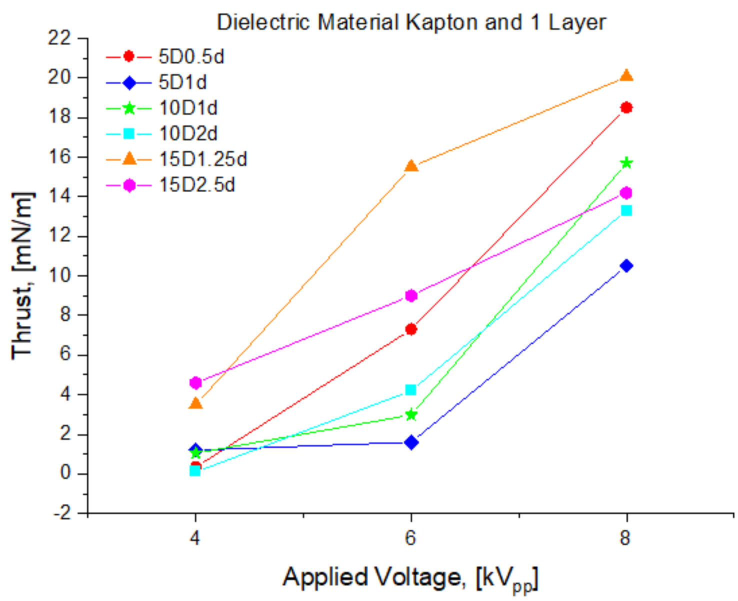

Figure 40. Thrust values of 1 layer sinusoidal geometry with different diameters

The graph in Figure 40 shows the thrust results of the DBD ion thrusters in the sinusoidal form in different diameters and amplitudes with Kapton layer number 1. Among these models, the highest thrust value is seen in the geoemtry with a diameter of 15 mm and an amplitude of 1.25. This highest value is about 20.05 mN/m. When all geometries with the same outer diameter, a decrease in the thrust results is observed with increasing amplitude of the sinusoidal geometry. One of the main reasons for this is that at smaller amplitudes produce more thrust which is related in a certain path that provides more collision forces of the ions in a narrower area (Gregory et al., 2007).

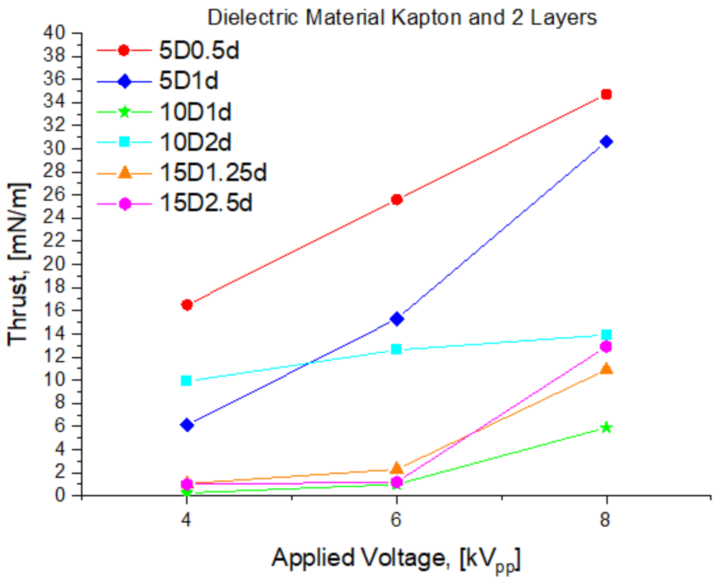

Figure 41. Thrust values of 2 layer sinusoidal geometry with different diameters

The thrust values of the DBD ion thruster with 2 layers of Kapton dielectric material at different diameters are as shown in Figure 41. When the Figure 41 is analyzed, the highest thrust value is the sinusoidal geometry with a diameter of 5D0.5d at a voltage value of 8 kV_{pp}. This value is about 34.7 mN/m.

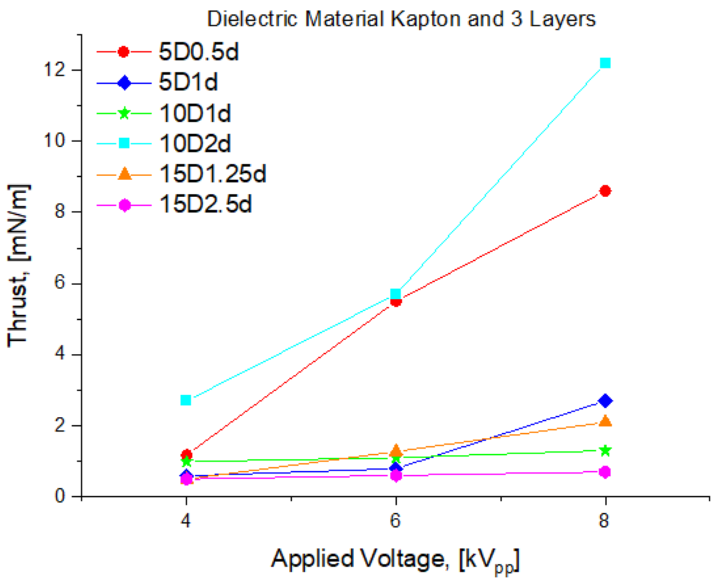

Figure 42. Thrust values of 3 layer sinusoidal geometry with different diameters

The graph in Figure 42 shows the thrust values of sinusoidal DBD ion thrusters having different diameters with 3 dielectric material layers. At 6 kV_{pp}, a significant decrease in the thrust value of the sine geometry with an outer diameter of 15 mm compared with other models. On this case, the highest thrust value is taken from 10D2d model at applied voltage value of 8kV_{pp}.

4.2. The Effects of Different Dielectric Material

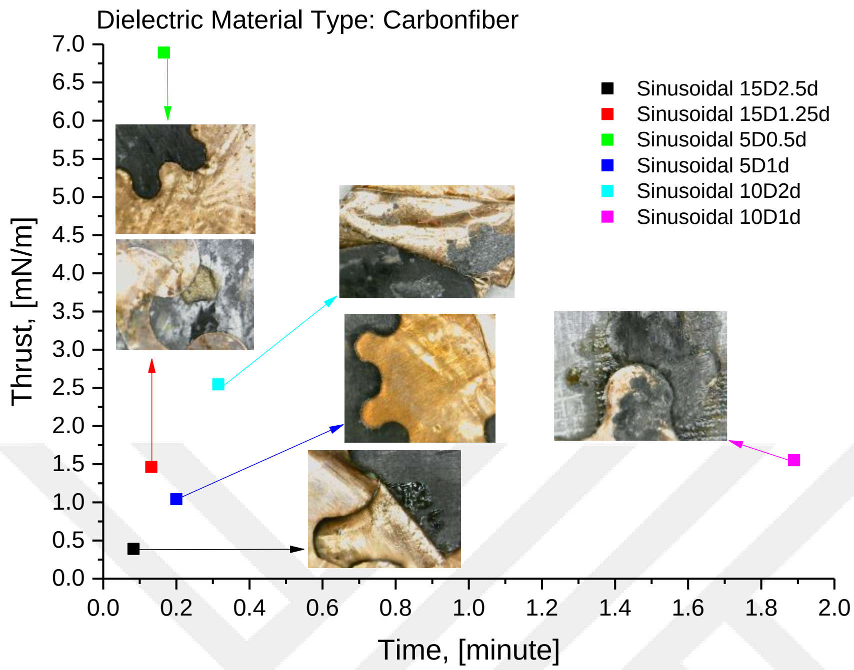

Figure 43. Thrust vs Lifecycle graph for sinusoidal ion thruster with Carbonfiber based dielectric material

Figure 43 shows the time-dependent thrust values of the DBD ion thrusters whose dielectric material was selected as carbonfiber. When the graph is examined, it is seen that the highest thrust value belongs to the DBD ion thruster with a sinusoidal 5D0.5d model. However, the ion thruster dielectric material is not sufficient in terms of life cycle. It was also observed that the thrust value of the DBD ion thruster with a diameter of 10D1d was not too high but life cycle of this ion thruster was the longest compared with other models. When the structure of the DBD plasma ion thrusters are examined in terms of material deformation, it is seen that both the dielectric material and the copper electrodes are damaged.

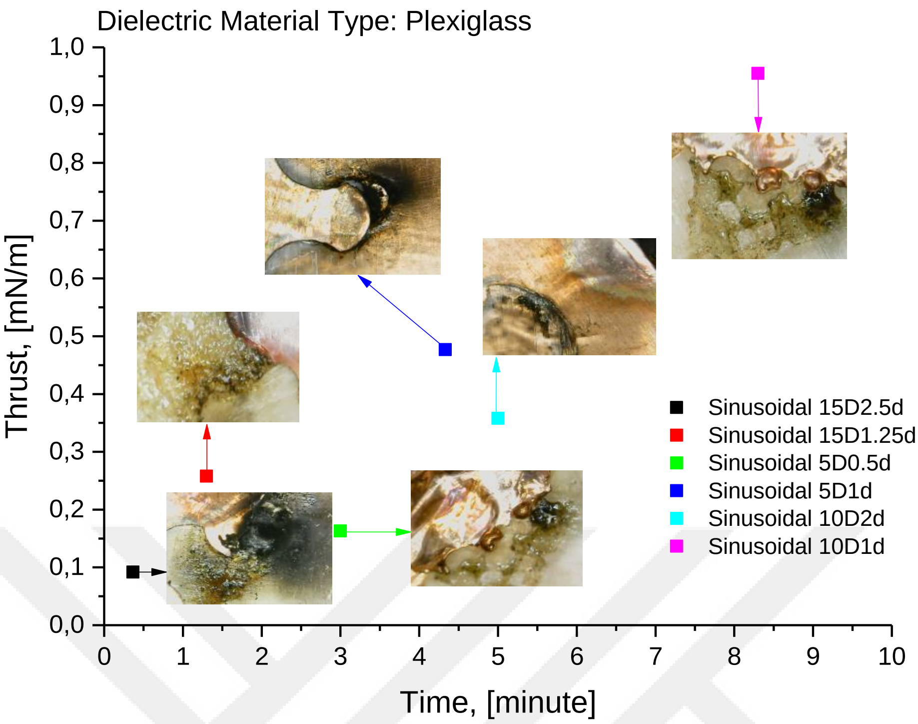

Figure 44. Thrust vs Lifecycle graph for sinusoidal ion thruster with Plexiglass based dielectric material

The graph in Figure 44 shows the time-dependent thrust values of the DBD ion thrusters whose dielectric material was selected as plexiglass. When the graph is examined, it is seen that the not only highest thrust value belongs to the DBD ion thruster with a sinusoidal 10D1d diameter but also life cycle of this thruster is longest. When the structure of the DBD plasma ion thrusters are examined in terms of material deformation, it is seen that both the dielectric material and the copper electrodes are damaged. Also, it appears that the geometries of the dielectric barrier discharge ion thrusters are deformed.

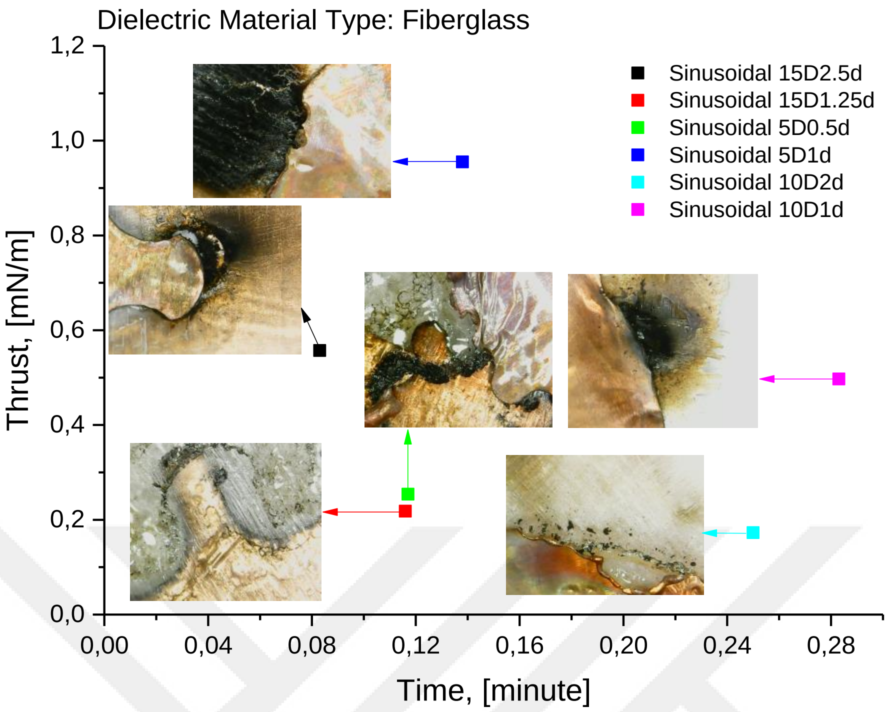

Figure 45. Thrust vs Lifecycle graph for sinusoidal ion thruster with Fiberglass based dielectric material

Figure 45 shows the time-dependent thrust values of the DBD ion thrusters whose dielectric material was selected as fiberglass. When the graph is examined, it is seen that the highest thrust value belongs to the DBD ion thrusters with sinusoidal 5D1d diameter, but the DBD ion thruster with 10D1d diameter has a higher life cycle compared with the other sinusoidal geometries.

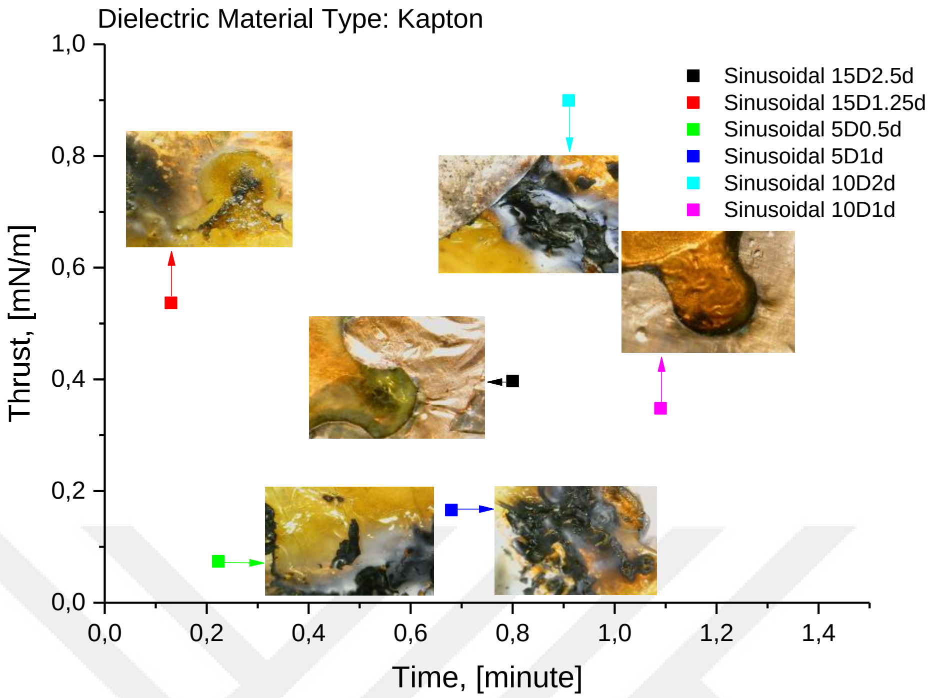

Figure 46. Thrust vs Lifecycle graph for sinusoidal ion thruster with Kapton based dielectric material

Figure 46 shows the time-dependent thrust values of the DBD ion thrusters whose dielectric material was chosen as kapton. When the graph is examined, it is seen that the highest thrust value belongs to the DBD ion thrusters with a sinusoidal 10D2d diameter, but the DBD ion thruster with a diameter of 10D1d has a higher thrust time between geometries with the same shape compared to other sinusoidal geometries. The thickness of each dielectric material are determined as 0.6mm, and the number of layers of the kapton dielectric material are set to be the same as this thickness.

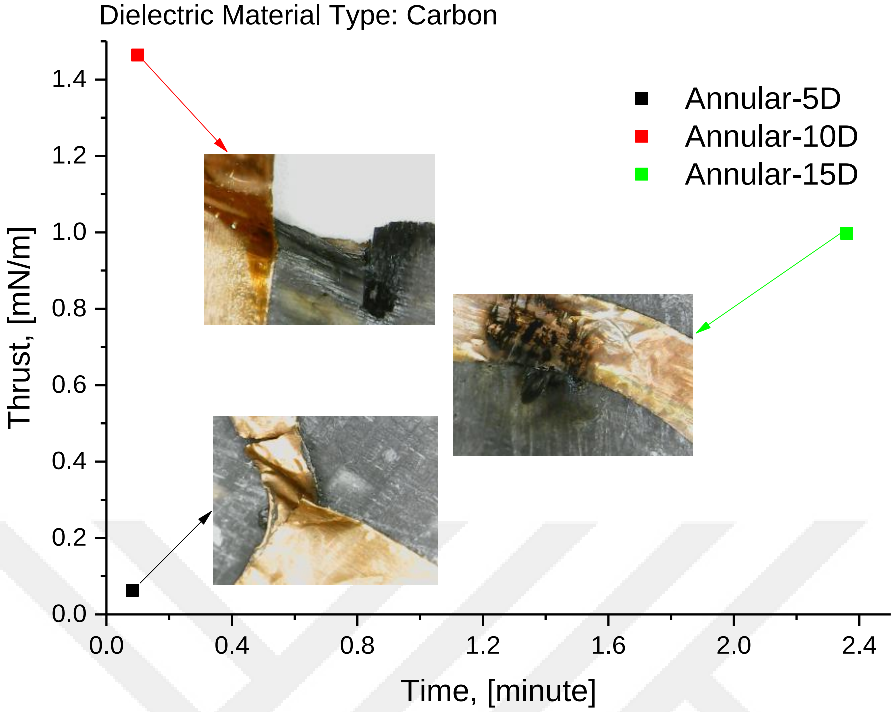

Figure 47. Thrust vs Lifecycle graph for annular ion thruster with Carbonfiber based dielectric material

Figure 47 shows the time-dependent thrust values of DBD ion thrusters with carbon fiber as the dielectric material. When the graph is analyzed, the highest thrust value belongs to the DBD ion thrusters with annular 10D diameter. The annular DBD ion thruster with 5D diameter produced lowest thrust. 15D annular base model has the highest life cycle. In this dielectric material based ion thruster structure, it appears that the dielectric material are less damaged than electrodes. In this plasma actuator type, it can be said that both electrode surfaces were damaged and the structure/geometry of the electrodes were disrupted.

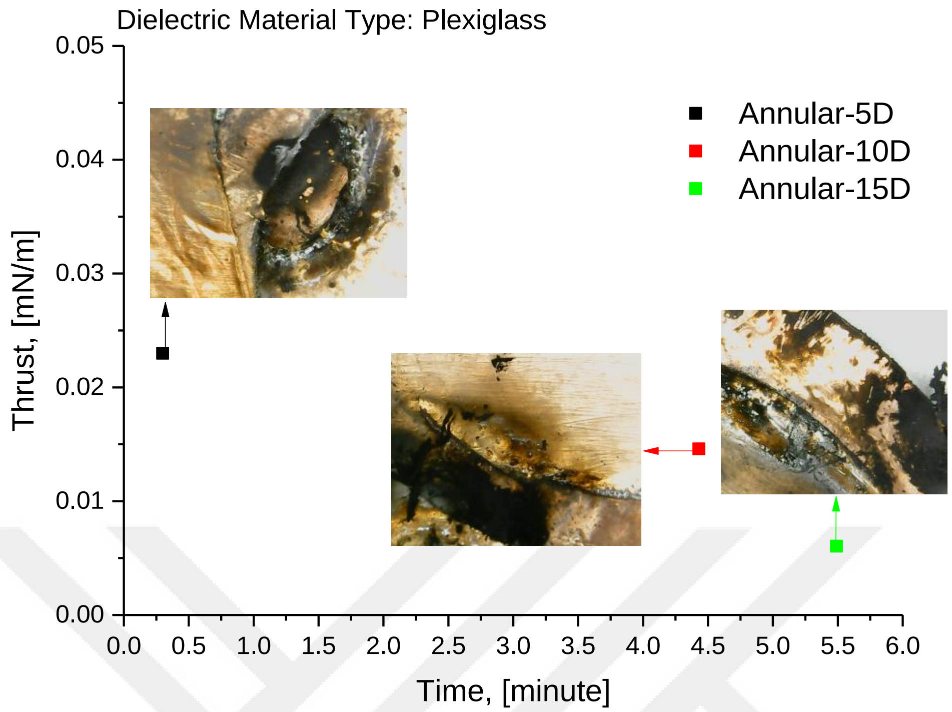

Figure 48. Thrust vs Lifecycle graph for annular ion thruster with Plexiglass based dielectric material

Figure 48 shows the time-dependent thrust values of DBD ion thrusters whose dielectric material was selected as plexiglass. The highest thrust value belongs to DBD ion thrusters with annular 5D diameter. Among the geometries with the same shape, the highest life cycle is observed with the DBD ion thruster with annular 15D model. Unlike the carbonfiber-based annular DBD ion thruster, it is seen that the structure of both the electrodes and the dielectric material is deteriorated in the plexiglass-based annular DBD ion thruster.

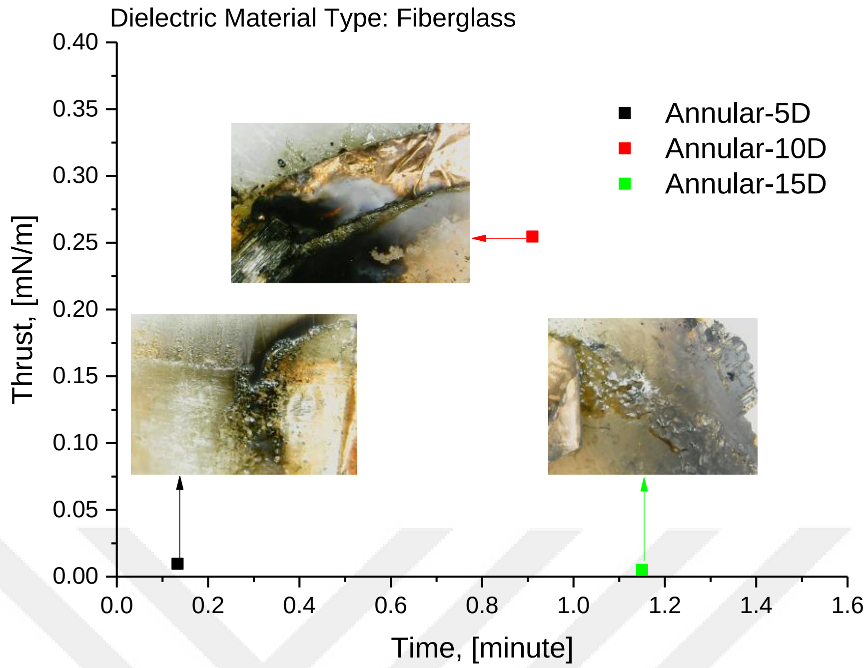

Figure 49. Thrust vs Lifecycle graph for annular ion thruster with Fiberglass based dielectric material

Figure 49 shows the time-dependent thrust values of DBD ion thrusters with fiberglass as the dielectric material. The highest thrust value belongs to DBD ion thrusters with annular 10D diameter. Among the geometries with the same shape, the lowest life cycle and thrust value is observed in the DBD ion thruster with annular 5D shape. The highest thrust value is observed in base annular DBD ion thruster 10D model. However, base annular DBD ion thruster 15D model has the longest life cycle. When the surface of the dielectric material of the 10D model DBD ion thruster is carefully examined, the bubbles caused degradation are clearly visible. These bubbles damage the dielectric material as a result of the energy charged by the molecules disintegrating into ions on the surface of the material. Especially as the application voltage increases, this energy level increases and the magnitude of the damage on the surface increases.

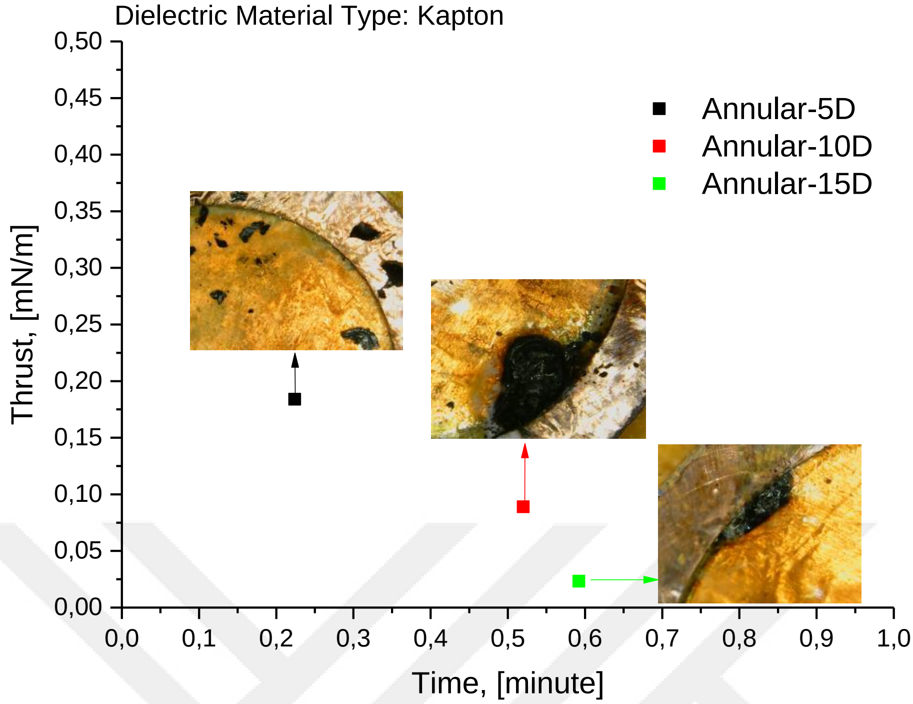

Figure 50. Thrust vs Lifecycle graph for annular ion thruster with Kapton based dielectric material

Figure 50 shows the time-dependent thrust values of DBD ion thrusters whose dielectric material was chosen as Kapton. When the graph is analyzed, it is seen that the highest thrust value and the lowest life cycle belongs to the annular DBD ion thrusters with 5D. The annular DBD ion thrusters with 15D has the longest life cycle and lower thrust value. When the surface of the Kapton dielectric material of the 5D model DBD ion thruster is carefully examined, in addition to the main degradation, partial degradation is observed in some regions. The main reason for this situation is that the production of the ion thruster is not done by machine and the air bubbles remain on the surface. It can be said that, unlike other dielectric material-based ion thrusters in this study, the electrodes of the Kapton dielectric-based ion thruster were not damaged too much.

5. CONCLUSIONS

Thrust performance of annular DBD plasma ion thrusters is examined in this thesis along with the influence of dielectric materials, dielectric material layer number, actuator geometry and applied voltage. The types of electric thrusters, annular DBD ion thrusters, and the history of the electric propulsion system are briefly described. Studies were conducted taking into account geometrical characteristics (sinusoidal and annular) to optimize the thrust of the ion thrusters considering electrical parameters, material types and kapton layers. 4 kV_{pp}, 6 kV_{pp}, and 8 kV_{pp} of voltage were applied in each experiment. The DBD plasma actuator's thrust was measured during the experiments by using an electrical thrust measurement device.

As a result of the thesis experiments, it is stated that the effectiveness of the thrust of the annular DBD ion thruster increases when the applied voltage is increased. Secondly, the thrust values of same geometries with large outer diameter varied while Kapton layer numbers are increased. Another of the main results of this thesis study, when all geometries with the same outer diameter are compared within themselves, a decrease in the thrust value is observed with increasing amplitude. One of the main reasons for this is that at smaller amplitudes, the collision forces of the ions in a narrower area are higher. Another finding of this thesis study is that the type of dielectric directly affects the thrust performance. Another finding is that the life cycles of the electrodes are directly related to the dielectric material in the structure of the electrodes. Dielectric material has a vital importance for space missions in determining the ion thruster which is having long life cycle or generating high thrust.

6. RECOMMENDATIONS

In the light of this thesis study results, following suggestions can be found for future studies;

- The excitation frequency variation on thrust performance of the annular DBD ion thruster can be investigated.
- The various geometrical parameters on thrust performance of the annular DBD ion thruster may be researched.
- Closeloop control application can be added to the annular DBD ion thruster.
- The thrust performance of the annular DBD ion thrusters may be tested under vacuum chamber.
- The various noble gases can be supplied to the annular type DBD ion thruster and their effects on thrust may be investigated.

REFERENCES

[1] Moreau E. (2007). ‘‘Airflow control by non-thermal plasma actuator’’, Journal of Phyics D: Applied Physics, 40, pp. 605-636.

[2] Akbıyık H., Yavuz H. and Akansu Y.E. (2018). ‘‘A study on the plasma actuator electrode geometry configurations for improvement of the aerodynamic performance of an airfoil’’, Strojniski Vestnik/Journal of Mechanical Engineering, 64, pp. 719-725.

[3] Benard N. and Moreau E. (2014). ‘‘Electrical and mechanical characteristics of surface AC dielectric barrier discharge plasma actuators applied to airflow control, Experiments in Fluids’’, 55, 1846, pp. 1-43.

[4] Stephen P. Wilkinson., E Siochi., Godfrey Sauti., Tian-Bing Xu., Maryann Meador and Hiaq. (2014). ‘‘Evaluation of dielectric-barrier-discharge actuator substrate materials’’, 45th American Institute of Aeronautics and Astronautics Plasmadynamics and Lasers Conference, 2810, pp. 1-29.

[5] A. Kosmodemyansky. (2000). ‘‘Konstantin Tsiolkovsky His Life and Work. University Press of the Pacific, Honolulu’’, Translated from the 1956 Russian text by X. Danko.

[6] Clary D.A. (2003). ‘‘Rocket Man: Robert H. Goddard and the Birth of the Space Age. Hyperion’.

[7] R.H. Goddard (1915). ‘‘Method and means for producing electrically-charged particles’’. US Patent No. 1,137,964.

[8] H. Oberth. Die Rakete zu den Planetenraumen (1923). ‘‘Druck und Verlag von R. Oldenbourg’’, Munich and Berlin.

[9] Ackeret J. (1947). ‘‘On the Theory of Rockets’’, Helvetica Physica Acta, pp.103–112.

[10] Langmuir I. (1913). ‘‘The effect of space charge and residual gases on thermoionic current in high vacuum’’, Physical Review, 192, pp. 450-486.

[11] Huang W., Kamhawi H. and Shastry R. (2012). “Farfield ion current density measurements before and after the NASA HiVHAc EDU2 vibration test”, 48th AIAA/ASME/SAE/ASEE Joint Propulsion Conference & Exhibit, Atlanta Georgia American Institute of Aeronautics and Astronautics , 4195, pp. 1-13.

[12] Choueiri E.Y. (2004). "A critical history of electric propulsion: The first 50 years’’, journal of propulsion and power, 20, pp. 193-203.

[13]NASA,C.A.,(2017).SolarSystem Exploration. https://solarsystem.nasa.gov/missions/deep-space-1/in-depth/

[14] Foing B.H., Racca G.D. and et al. (2003). ‘‘SMART-1 mission to the moon: technology and science goals’’, Advance in Space Research , 31, 11, pp. 2323-2333,.

[15] Goebel D.M and Katz I. (2008). ‘‘Fundamentals of electric propulsion: ion and hall thrusters’’, Jet Propulsion Laboratory California Institute of Technology, pp. 1-507.

[16] Borghi C.A., Carraro M.R., Cristofolini A. and Neretti G. (2008). ‘‘Electrohydrodynamic interaction induced by a dielectric barrier discharge’’, Journal of Applied Physics, 103, 063304, pp. 1-11.

[17] Van Dyken R., McLaughlin T.E. and Enloe C.L. (2004). ‘‘Parametric investigations of a single dielectric barrier plasma actuator’’, 42nd AIAA Aerospace Sciences Meeting and Exhibit, 846, pp. 1-12.

[18] Correale G., Winkel R. and Kotsonis M. (2015). ‘‘Energy deposition characteristics of nansecond dielectric barrier discharge plasma actuators: influence of dielectric material’’, Journal of Applied Physics, 118, 083301, pp. 1-13.

[19] Roslı M.F.A.B. (2022). ‘‘Experımental study on the impact of DBD plasma actuator geometry and electrical input on thrust generation’’, Doctoral Dissertation Universiti Sains Malaysia, pp. 1-36.

[20] Abdollahzadeh M., Pascoa, J.C. and Oliveira P. J. (2014). ‘‘Modified split-potential model for modeling the effect of DBD plasma actuators in high altitude flow control’’, Current Applied Physics, 14, 1160, pp. 1-24.

[21] Mora E.Y., Sarmiento A. and Vera E. (2016). ‘‘Alumina and quartz as dielectrics in a dielectric barrier discharges DBD system for CO2 hydrogenation’’, In Journal of Physics: Conference Series , 687, 012020, pp. 1-5.

[22] Bellan P.M. (2008). ‘‘Fundamentals of plasma physics’’, Cambridge University Press.

[23] Langmuir I. (1919). ‘‘The arrangement of electrons in atoms and molecules’’, Journal of the American Chemical Society, 41, pp. 868-934.

[24] Bansal J.L. (1994). ‘‘Magnetofluiddynamics of viscous fluids india’’, Jaipur Publishing House, pp. 1-361.

[25] Li W. and Hudson M.K. (2019). ‘‘Earth's van allen radiation belts: from discovery to the van allen probes era’’, Journal of Geophysical Research: Space Physics, 124, pp. 8319–8351.

[26] Jahn R.G. and Choueiri E.Y. (2003). "Electric propulsion", Encyclopedia of Physical Science and Technology, pp. 125–141.

[27] Borghi C.A., Carraro A., Cristofolini A. and Neretti G. (2008). ‘‘Electrohydrodynamic interaction induced by a dielectric barrier discharge’’. Journal of Applied Physics, pp. 103-111.

[28] Borghi C.A., Cristofolini A., Neretti G., Seri P., Rossetti A., and Talamelli A. (2017). ’’Duty cycle and directional jet effects of a plasma actuator on the flow control around a NACA0015 airfoil’’, Meccanica, 52, pp. 3661-3674.

[29] Cristofolini A., Neretti G., Roveda F. and Borghi C.A. (2012). “Schlieren imaging in a dielectric barrier discharge actuator for airflow control”, Journal of Applied Physics, 111, 033302.

[30] Hoskinson A.R., Hershkowitz N. and Ashpis D.E. (2008). “Force measurement of single and double barrier DBD plasma actuators in quiescent air”, Journal of Physics D:Applied Physics, 41, 245209.

[31] Shin J. and Raja L.L. (2007). ‘‘Run-to-run variations, asymmetric pulses and long time-scale transient phenomena in dielectric-barrier atmospheric pressure glow discharges’’, Journal of Applied Physics, pp. 1-18.

[32] Komuro A., Takashima K., Konno K., Tanaka N., Nonomura T., Kaneko T., Ando A., and Asai K. (2017). “Schlieren visualization of flow-field modification over an airfoil by near-surface gas-density perturbations generated by a nanosecond-pulse-driven plasma actuator”, Journal of Applied Physics, 50, 215202, pp. 1-11.

[33] Thomas F.O., Corke T.C., Iqbal M., Kozlov A. and Schatzman D. (2009). ‘‘Optimization of dielectric barrier discharge plasma actuators for active aerodynamic flow control’’, American Institute of Aeronautics and Astronautics, 47, pp. 2169-2178.

[34] Ashpis D.E. and Laun M.C. (2014). ‘‘Dielectric barrier discharge (DBD) plasma actuators thrust-measurement methodology incorporating new anti-thrust hypothesis’’, In 52nd Aerospace Sciences Meeting.

[35] Vernet J., Örlü R. and Alfredsson P.H. (2015). “Separation control by means of plasma actuation on a half clinder approach by a turbulent boundary layer”, Journal of Wind Engineering and Industrial Aerodynamics, 145, pp. 318-326.

[36] Akbıyık H., Yavuz H. and Akansu Y.E. (2017). ‘‘Comparison of the linear and spanwise-segmented DBD plasma actuators on flow control around a NACA0015 airfoil’’, IEEE Transactions On Plasma Science, 45, pp. 2913-2921.

[37] Riherd M. and Roy S. (2013). ‘‘Serpentine geometry plasma actuators for flow control’’ Journal Of Applied Physics, pp. 114-115.

[38] Zhou L., Wei L., Zhou D., Zhu X., Li H., and Yu D. (2022). ‘‘The characteristics of ion wind thruster based on dielectric barrier discharge in near space’’, Vacuum, 195, 1-10.

[39] Chabert, P., Arancibia Monreal, J., Bredin, J., Popelier, L., & Aanesland, A. (2012). ‘‘Global model of a gridded-ion thruster powered by a radiofrequency inductive coil’’, Physics of Plasmas, 073512, pp. 1-7.

[40] Craig S., Humble R., Hofferth J. and Saric W. (2011). ‘‘Characterization of the Flowfield Structure of an Annular Dielectric Barrier Discharge Plasma Actuator’’, American Institute of Aeronautics and Astronautics, 3987, pp. 1-9.

[41] Humble R.A., Craig S.A., Vadyak J., McClure P.D., Hofferth J.W. and Saric W.S. (2013). "Spatiotemporal structure of a milimetric annular dielectric barrier discharge plasma actuator", Physics of Fluids, 25, 017103, pp. 1-22.

[42] Neretti G. (2017). ''Geometry optimization of linear and annular plasma synthetic jet actuators'', Journal of Applied Physics, pp. 1-9.

[43] Neretti, G. (2018). ''Measurement of the charge distribution deposited by an annular plasma synthetic jet actuator over a target surface'', Journal of Applied Physics, 324004, pp. 1-9.

[44] McGowan R., Corke T.C. and Matlis E. (2016). ''Pulsed-dc plasma actuator characteristics and application in compressor stall control''. American Institute of Aeronautics and Astronautics SciTech Forum, pp. 1-15.

[45] Gregory J.W., Enloe C.L., Font G.I. and Mclaughlin T.E. (2007). ''Force production mechanisms of a dielectric barrier discharge plasma actuator'', American Institute of Aeronautics and Astronautics, pp. 1-13.

[46] Coleman H.W., Steele W.G. and Brown K.K. (1997). ''A methodology for determining experimental uncertainties in regressions'', Journal of Fluid Engineering, 120, pp. 445-456.

APPENDIX

In this study, the uncertainty values of the measured and calculated parameters were determined by the methods presented by Coleman and Steele (1998). The experimental parameters are functions of the form of equation E-1.

$$r = kX_1^a X_2^b X_3^c \dots \quad \text{(E.1)}$$

The uncertainty expression of the function in this form is expressed in equation E-2.

$$u_r = \frac{w_r}{r} = \left[a^2(u_{x_1})^2 + b^2(u_{x_2})^2 + c^2(u_{x_3})^2 + \cdots\right]^{1/2} \quad \text{(E.2)}$$

Within the scope of this study, parameters such as thrust measuring device, application voltage, release frequency, ion thruster production geometry, ion thruster holder apparatus, etc. were measured experimentally and calculated for the thrust value using these measurement results.

- In a 200 g thrust measurement, an error of 0.01 g can occur. In this case, the uncertainty of the thrust measuring device is 0.005%.
- An error of 100 Vpp can occur in setting the application voltage of 14000 Vpp. In this case, the uncertainty in setting the application voltage is 0.71%.
- An error of 10 Hz may occur in setting the release frequency of 5500 Hz. In this case, the uncertainty in setting the release frequency is 0.18%.
- Setting the 20 mm ion thruster geometry may result in a 0.5 mm placement error. In this case, the uncertainty in setting the ion thruster geometry is obtained as 2.5%.
  A 0.1 mm error can occur in adjusting the length of the holder apparatus of the 15 mm ion thruster. In this case, the uncertainty in adjusting the length of the ion thruster holder is 0.6%.

Taking these uncertainties into account, the total uncertainty in the velocity measurement;

$$u_{F_{thrust}} = \frac{w_{F_{thrust}}}{F_{thrust}} = \left[\left(\frac{w_{X_1}}{X_1}\right)^2 + \left(\frac{w_{X_2}}{X_2}\right)^2 + \left(\frac{w_{X_3}}{X_3}\right)^2 + \left(\frac{w_{X_4}}{X_4}\right)^2 + \left(\frac{w_{X_5}}{X_5}\right)^2\right]^{1/2}$$

$$u_{F_{thrust}} = \frac{w_{F_{thrust}}}{F_{thrust}} = \left[(0.00005)^2 + (0.0071)^2 + (0.00018)^2 + (0.025)^2 + (0.0006)^2\right]^{1/2} \cong 0.051$$

In general, 2.6% was obtained in the thrust measurement.